FORCE POTENTIATION IN THE MDX MOUSE

IAN CURTIS SMITH, BSc.

A thesis submitted in partial fulfillment of the requirements for

the degree of Master of Science in Applied Health Sciences

Supervisors: Dr. Rene Vandenboom, Dr. A. Russell Tupling

Faculty of Applied Health Sciences
Brock University
500 Glenridge Ave.
St. Catharines, ON
L2S 3A1

Abstract:

Large forces are the primary mechanism of injury in muscular dystrophy, and muscular dystrophy is especially damaging to type IIB muscle fibers. It was hypothesized that post-tetanic potentiation (PTP) would be down-regulated to prevent damage in X-linked muscular dystrophy (*mdx*) mice since PTP increases force and PTP effects are greatest in IIB fibers. PTP experiments were performed on the extensor digitorum longus (EDL) of 50 day old *mdx* (YM) and C57BL/10 (YC) mice and 10 month old *mdx* (OM) and C57BL/10 (OC) mice. Twitch and tetanic forces were lower in *mdx* than controls and lower in younger than older mice. Contrary to the hypothesis, PTP was higher in both *mdx* groups compared to controls. OM potentiated more than any other condition (OM: 29.8%, OC: 23.2%, YM: 21.9%, YC: 17.2%). In accordance with literature PTP increased in the older groups. To explain PTP changes, fiber typing and Western blots for myosin light chain kinase (MLCK) were performed. YM and YC had similar fiber type profiles (2% I, 58% IIX/D and 40% IIB). In accordance with literature but contrary to expected conditions for elevated PTP, OM had a slower fiber type profile (1.7% I, 69% IIX/D and 29% IIB) than OC (0.4% I, 61% IIX/D and 38% IIB). No differences were found in MLCK expression. It seems that PTP is up-regulated to maintain muscle function rather than being down-regulated to prevent muscle damage. Ca^{2+} transient and myosin phosphorylation measurements would be beneficial in explaining increased PTP seen in this study.

Acknowledgements:

A big thank you goes out to Dr. Russell Tupling and Dr. Rene Vandenboom for their guidance and support in this endeavor. I would also like to thank Dr. Brian Roy and Dr. Dennis Claflin for their advice on this project.

I also appreciate the help of my lab mates and coworkers who were always available to lend a hand or a kick in the right direction. Eric Bombardier deserves a specific thank you for his guidance on tissue cutting and staining.

Matthew Ramer and Guillaume Couillard, thanks to both of you for helping me count cells (even though I had to do a full recount).

I would also like to thank the support staff at both Brock University and the University of Waterloo for their help. Research would be much harder without them.

Thank you to the Canadian Institute of Health Research for funding this project.

The mice used in this study gave their lives to advance scientific knowledge and it should not go unnoticed.

Finally I would like to thank my friends and family who played a more intangible role as I worked through this project. Your love and support got me through more obstacles than you know.

Happiness and success to you all.

Table of Contents

List of Figures

List of Tables

List of Abbreviations

ADP - Adenosine diphosphate

α_{FS} - Fraction of crossbridges in the force producing state

ASI - Aurora Scientific Inc.

ATP - Adenosine triphosphate

Ca^{2+} - Calcium

$[Ca^{2+}]_c$ - Concentration of cytosolic calcium

CaM - Calmodulin

CO_2 - Carbon dioxide gas

CS - Conditioning stimulus

CSA - Cross sectional area

$+df/dt$ - Rate of force production

$-df/dt$ - Rate of relaxation

DMD - Duchenne muscular dystrophy

EDL - Extensor digitorum longus

f_{app} - Transition from the non-force producing state to the force producing state

FDB - Flexor digitorum brevis

g_{app} - Transition from the force producing state to the non-force producing state

HMM - Heavy meromyosin

LC - Light chain

LC2f - Fast twitch skeletal muscle isoform of the myosin regulatory light chain

LC2s - Slow twitch skeletal muscle isoform of the myosin regulatory light chain

LFF - Low frequency fatigue

LMM - Light meromyosin

mdx - X-linked muscular dystrophy

MLCK - Myosin light chain kinase

MVC - Maximum voluntary contraction

n - Number of samples

O_2 - Oxygen gas

OC - 10 month old C57BL/10 mice

OM - 10 month old *mdx* mice

PAP - Post-activation potentiation

pCa - – log (calcium concentration)

P_o - Absolute tetanic force

$PP1_\beta$ - Protein phosphatase subunit β

$PP1_M$ - Myosin regulatory light chain protein phosphatase

P_t - Absolute twitch force

PTP - Post-tetanic potentiation

RLC - Regulatory light chain

1/2RT - Half relaxation time

S1 - Myosin subfragment 1

S2 - Myosin subfragment 2

SE - Standard error of the mean

SERCA - Sarco/endoplasmic reticulum calcium ATPase

skMLCK - Skeletal muscle myosin light chain kinase

smMLCK - Smooth muscle myosin light chain kinase

SR - Sarcoplasmic reticulum

TnC - Troponin C

TPT - Time to peak tension

YC - 50 day old C57BL/10 mice

YM - 50 day old *mdx* mice

Chapter 1

Introduction:

Duchenne muscular dystrophy (DMD) is an X-linked myopathy affecting one in 3500 live male births, and normally leads to death in the second or early in the third decade of life by respiratory or cardiac failure. The X-linked muscular dystrophy (*mdx*) mouse is the most commonly used animal model of DMD.

The primary dysfunction in DMD and *mdx* mice is lack of the costameric protein dystrophin (14). Dystrophin acts to stabilize and support the sarcolemma. Without dystrophin, the sarcolemma is especially vulnerable to damage induced by forceful contractions (20; 31; 50; 78), but not repetitive low force contractions (78). Due to larger cross sectional area, the ratio of force to surface area of an individual fiber is larger in faster fibers than slower fibers. This leads to more force being transferred through the sarcolemma per unit of area. Therefore each individual twitch will be more damaging to the sarcolemma in a faster fiber than a slower fiber. Additionally, slow fibers have the protein utrophin which can help stabilize the dystrophin complex, preventing some damage to the sarcolemma (18; 19). As such, faster fibers are affected to a greater extent by *mdx* and DMD (5; 21; 79; 112).

Microscopy studies suggest that the life of an *mdx* mouse can be divided into four distinct stages. The first stage lasts up to 3 weeks after birth. In this stage the *mdx* mouse shows no differences in fiber size, degree of fiber damage or fiber type from control mice (28; 53). From 3-4 weeks after birth, *mdx* mice experience a period of massive fiber degeneration. During this period, muscle fibers show branching, super-contracted regions, and cores of necrotic fibers (44; 115). Following this degenerative period there is

a regenerative period where satellite cells form new cells and repair damaged fibers (53). During this time *mdx* mice show increased muscle hypertrophy compared to control mice, but these large muscles are weaker (60; 61; 97; 100). The end of the regenerative period occurs between 4 and 6 months of age and is marked by a complete lack of expression of embryonic myosin, indicating the presence of only mature, differentiated muscle fibers (21; 79). After 6 months of age, *mdx* mice lose body mass linearly until 2 years of age (60). During this degenerative period, the content of connective tissue and fat in muscle increases (60; 61; 97; 100), and the proportion of type IIB fibers slowly declines to zero (21).

Muscle can be activated by previous contractile activity. This occurs when the regulatory light chain (RLC) of myosin is phosphorylated by myosin light chain kinase (MLCK) (110). This phosphorylation serves two purposes: to increase the amount of force produced at any given submaximal concentration of cytosolic calcium ($[Ca^{2+}]_c$) and to increase the maximum amount of power the muscle can produce via increased rate of force development ($+df/dt$) (108). In rodent muscle, myosin phosphorylation readily occurs in type IIB fibers, but is more difficult to induce in type IIA fibers and even more so in type I fibers (65; 74; 75). Individual rodent muscles have more homogeneous fiber type distribution than humans. Accordingly, different muscles show different degrees of force potentiation based on their primary fiber type composition. Muscles composed primarily of IIB fibers such as the lumbrical, flexor digitorum brevis and extensor digitorum longus (EDL) exhibit greater potentiation than muscles mainly comprised of IIA fibers such as the diaphragm (49; 65; 74; 75).

It is possible that RLC phosphorylation plays a role in the increased damage seen in diaphragm of *mdx* mice compared to other skeletal muscles. The diaphragm has a much higher workload than other skeletal muscles, with a respiration rate of 200 breaths per minute (29; 97) and a stimulation frequency within each breath that can reach up to 100 Hz (47; 66). This high workload may provide enough stimulation to show net phosphorylation of the slower fiber types, thereby increasing the force for a given Ca^{2+} release and providing opportunity for increased damage to the sarcolemma. Over the course of a lifetime, this could help explain why there is an overall loss of sarcomeres seen in the diaphragm that is not seen in other muscles (97).

Anderson, Bressler and Ovalle (5) have performed a study examining force potentiation in dystrophic muscle. The investigators examined post-tetanic potentiation (PTP) in soleus and EDL muscles of *mdx* and control mice at 4 and 32 weeks of age. They report no differences in potentiation between *mdx* and control animals or between the ages examined. However, at both ages they reported significantly lower content of phosphorylated RLC at rest in EDL expressed as a proportion of all myosin light chains present in the muscle. This was not measured in soleus or following muscular contraction. This work was performed before the roles of the different light chains had been determined. As such, it is possible that changes in expression of myosin light chains other than the RLC had masked the true changes in RLC phosphorylation.

Chapter 2

Review of Literature:

I. Potentiation:

The amount of force a muscle is able to produce depends on two factors: the number of cross bridges in the strongly attached state and the force produced per cross-bridge. While the force produced per cross-bridge is relatively consistent from sarcomere to sarcomere and muscle to muscle, the number of cross-bridges formed varies greatly. Steric modeling has shown that in an isometric contraction, the number of crossbridges in the strongly attached state may reach as high as 3 per 7 actin monomers (59). Survival is dependent on the efficient modification of muscle forces. As such, crossbridge binding is subject to a great deal of regulation that can optimize and amplify the force output for a given excitation. One regulatory mechanism is the potentiation of muscle forces. Potentiation is a temporary increase in both the isometric twitch force and *df/dt* caused by previous contraction of a muscle (1; 62). Potentiation following voluntary contractions is known as post-activation potentiation (PAP) (55; 62), and potentiation following tetanic stimulation is PTP (55; 65; 74). Progressive increases in twitch force during low frequency stimulation are known as staircase potentiation (55). The rate of phosphorylation is slow compared to the rate of contraction. The first second of a muscular contraction causes very little phosphorylation (reviewed in (101)). PAP and PTP are generally highest 20-30 seconds following the invoking contraction, and decay exponentially within a few minutes of inactivity (49; 108).

II. Mechanisms of Potentiation:

The myosin protein contains two regions, a coiled coil region that spans much of its length, known as the myosin rod, and a large globular region at the NH_2-terminus, termed the head or subfragment 1 (S1) (see figure 2.1). A portion of each myosin rod, the light meromyosin (LMM), interacts with the LMM of other myosin proteins forming the myosin backbone. Heavy meromyosin (HMM), comprised of the remainder of the myosin rod, (subfragment 2, or S2) and the S1 head, projects from the myosin backbone (reviewed in (38)). The joints between S1 and S2 and HMM and LMM are flexible. These joints are important for force production as the angle of S1 changes according to nucleotide binding state. The HMM-LMM junction is a regulatory site for the myosin regulatory light chain (RLC), which is located near the base of S2 (70). For muscle to contract following an action potential, Ca^{2+} must be released from the sarcoplasmic reticulum (SR) causing the cytosolic calcium concentration ($[Ca^{2+}]_c$) to increase. Ca^{2+} binds to troponin C, causing tropomyosin to roll off the myosin binding sites on actin, allowing the formation of strong crossbridges and force production.

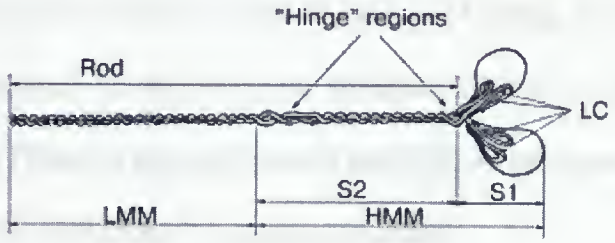

Figure 2.1: Reproduced from Levitsky, 2004 (58). Schematic representation of myosin and its fragments: S1, myosin subfragment 1; S2, myosin subfragment 2; HMM, heavy meromyosin; LMM, light meromyosin; LC, light chains; Rod, rod part of the molecule.

The low α-helix content in the "hinge" regions allows more mobility than in the remainder of the rod region.

Force potentiation is the result of increased Ca^{2+} sensitivity caused by phosphorylation of the myosin regulatory light chains (RLC) by myosin light chain kinase (MLCK) (110). Two isoforms of MLCK are expressed in skeletal muscle: skeletal muscle MLCK (skMLCK) and smooth muscle MLCK (smMLCK). The DNA encoding MLCK is found on chromosome 3 in humans (34) and chromosome 16 in mice (35). The skMLCK isoform appears to be the functionally important isoform in skeletal muscle, as smMLCK does not phosphorylate the RLCs of skeletal muscle. It is thought that the RLCs of skeletal muscle are poor substrates for smMLCK because of a substitution of arginine for glutamine near the phosphorylation site (118). The active site that phosphorylates the RLC is partially blocked by a binding site for calmodulin (CaM). CaM is bound to the CaM binding site on MLCK when $[Ca^{2+}]_c$ is high. Four Ca^{2+} ions bind cooperatively to CaM causing structural changes, causing it to become more compact and allowing it to bind to the CaM binding site, freeing the active site for RLC phosphorylation on MLCK. In the absence of inhibition, MLCK modulates the activity of myosin ATPase by phosphorylating the RLC on the myosin head, a process requiring the cleavage of ATP to ADP (reviewed in (101)).

Phosphorylation can be described as a two state model: a force producing state and a non-force producing state. The transition from the non force producing state to the force producing state can be described as f_{app} and the transition from the force producing state to the non-force producing state can be described as g_{app}. The fraction of

crossbridges in the force producing state is designated α_{Fs}. The force produced at any given level of excitation is proportional to α_{Fs}, and can be expressed as $\alpha_{Fs} = f_{app} / (f_{app}+g_{app})$ (11; 102; 108). Adding a phosphate group adds two negative charges to the RLC of HMM (39; 70). This causes the average position of HMM to shift away from the negatively charged LMM towards the thin filament (39; 62; 70). The closer association of actin and the S1 head increases the likelihood of their interaction and crossbridge formation at any given concentration of Ca^{2+} and this increases f_{app} (11; 102; 108). In instances when myosin and actin are already closely associated, such as at long muscle lengths, RLC phosphorylation has no added effect on f_{app} (81). $[Ca^{2+}]_c$ and RLC phosphorylation do not affect g_{app}. RLC phosphorylation has the effect of increasing f_{app} at all $[Ca^{2+}]_c$. It is this single mechanism that accounts for the increased forces seen at non-saturating Ca^{2+} concentrations and the increased $+df/dt$ seen in potentiated muscle (11; 102; 108). At low $[Ca^{2+}]_c$, f_{app} is low, but due to the closer association of myosin to actin when the RLC is phosphorylated, f_{app} is increased and greater forces can be produced, as the fraction of crossbridges in the force generation phase is higher (11; 102; 108). At high $[Ca^{2+}]_c$, g_{app} is very small compared to f_{app} , causing α_{Fs} to approach 1.0, meaning essentially all available myosin binding sites have crossbridges in the force generating state, resulting in no further force increases (11; 102; 108). This reflects the sigmoidal relationship of the force-pCa curve (4). The rate of force development is a function of f_{app}. The increases in f_{app} over unpotentiated muscle at any given $[Ca^{2+}]_c$ are directly proportional to the phosphorylated RLC content, and thus increases in the rates of force development are graded to the differences in phosphorylation content through its influence on f_{app} (11; 102; 108).

When $[Ca^{2+}]_c$ drops through Ca^{2+} uptake into the SR, Ca^{2+} dissociates from CaM, which then reverts to its original conformation, blocking the RLC binding site on MLCK preventing further phosphorylation. Myofibrillar protein phosphatase type 1 ($PP1_M$) removes the phosphate group from the light chain and myosin is deactivated as HMM associates more closely with the protein backbone (reviewed in (101)).

Recent evidence has suggested that there are other mechanisms involved in potentiation that do not involve phosphorylation of the RLC. Zhi *et al.* (118) have shown that there is a low basal amount of RLC phosphorylation in skMLCK knockout mice, ~0.05 mol phosphate/mol RLC. These mice do not show PTP, but do show staircase potentiation at 10 Hz in the EDL, with a relative increase in twitch force of 1.35 (1.55 in wild type) after 15 seconds of staircase. This is not due to increased activity of another kinase, as phosphorylated RLC content did not increase over basal levels. This potentiation was hypothesized to be due to the effects of prolonged repetitive release of Ca^{2+}. Increased $[Ca^{2+}]_c$ results in Ca^{2+} binding to troponin C (TnC) and activation of the thin filament through the allosteric effects of TnC (87; 118). The rate of dissociation of Ca^{2+} from TnC is much slower than the rate of Ca^{2+} binding (87). Results from Jiang and Julian (51) report a "bump" in the fluorescence signal during muscle relaxation in tibialis anterior fibers from the frog *Rana temporaria.* This bump was shown to be mass unloading of Ca^{2+} from TnC due to lost crossbridge-Ca^{2+} binding cooperativity effects following crossbridge release. It therefore seems unlikely that Ca^{2+} can remain bound to TnC in situations that do not involve summation of forces.

A second mechanism proposed to explain staircase potentiation in skMLCK knockouts was that compression of the myofilament lattice could occur, reducing the

spacing between actin and myosin, mimicking the effects of RLC phosphorylation (38; 62; 101; 118). Based on results from slack tests of intact tibialis anterior fibers from *Rana temporaria,* this seems unlikely. Lattice spacing takes ~35 ms to reach maximum spacing following muscle release, but takes over 200 ms to compress to a new set point following the onset of tension redevelopment (17). Since lattice compression takes much longer than expansion, and twitches occur every 100 ms (10 Hz), there should be only transient changes in lattice spacing, as the lattice has ample time to expand after each twitch. . Repetitive Ca^{2+} release can result in Ca^{2+} binding to CaM due to its slow Ca^{2+} release kinetics (101).

A third suggestion to explain staircase potentiation in skMLCK knockouts was a suggestion that CaM binding to dihydropyridine and ryanodine receptors will affect excitation characteristics, however, the Ca^{2+}-CaM complex inhibits dihydropyridine and ryanodine receptors, while the unbound protein is an activator (41). It therefore seems unlikely that Ca^{2+} release will increase during staircase. A more likely cause of staircase potentiation may be an increase in the basal levels of Ca^{2+}. Fast contraction-relaxation cycling may not allow enough time for Ca^{2+} to be fully removed from the cytosol leading to progressively higher cytosolic Ca^{2+} levels, more saturated Ca^{2+} buffers allowing twitch forces to progressively increase. However, both increased peak and resting $[Ca2+]_c$ have been documented in isolated mouse EDL (25).

III. Potentiation in Fiber Types:

Two isoforms of RLC are expressed in skeletal muscle: LC2f and LC2s. While both isoforms are expressed in fast and slow fibers, LC2f is expressed to a higher extent

in fast fibers, while LC2s is more highly expressed in slow fibers (36). The expression of these proteins appears to be based on neural input. Bozzo *et al.* (10) denervated the soleus and EDL in one limb of rats and discovered that the amount of LC2s decreased relative to LC2f in soleus when compared to control animals and the contra lateral leg. There were no differences seen in LC2 content of EDL. There are two phosphorylation sites on the RLC (36; 45). In resting muscle there is a basal level of phosphorylation (45; 110; 118). This basal level of phosphorylation is seen in skMLCK knockout mice to a much lower extent (118). There are currently no studies examining the functional effects of dual phosphorylation versus monophosphorylation in skeletal muscle, or if skMLCK is responsible for phosphorylation of both sites.

Unlike in smooth muscle, RLC phosphorylation is non-essential to skeletal muscle contraction, but instead acts as a modifier (64). As such, skMLCK activity is different in different fiber types. Potentiation effects are highest in fast glycolytic fibers (type IIB, IIX/D), followed by fast oxidative glycolytic fibers (type IIA) and lowest in slow oxidative fibers (type I). This has been shown in a variety of human and animal models (49; 65; 74; 75). Accordingly, when compared to type I fibers, the MLCK activity is 3.4 and 1.5 times higher in type IIX/D and type IIA respectively (75). Previous contractile activity does not result in increased twitch force or marked increase in RLC phosphorylation in type I fibers, and may represent a basal degree of phosphorylation (49; 65; 74; 75). However, the rate constant of dephosphorylation has been shown to be four times larger in slow oxidative fibers than fast glycolytic fibers, indicating differences in phosphatase 1 activity (75). A study by Bozzo *et al.* (10) points to neural input as a key regulator of MLCK expression. Denervation of rat soleus results in increased skMLCK

expression and more basal phosphorylation in both LC2s and LC2f. Following denervation of EDL, the concentration of skMLCK is decreased, and basal phosphorylation is decreased in LC2s but not LC2f. Chronic low frequency stimulation of EDL results in reduced skMLCK expression and less basal phosphorylation in both RLC isoforms. Protein phosphatase 1 ($PP1_M$) expression was not affected by any of these stimuli.

IV: Functional Benefits of Potentiation:

RLC phosphorylation does not exclusively increase force production in isometric contractions, as submaximal dynamic contractions also exhibit greater Ca^{2+} sensitivity with RLC phosphorylation (40). Potentiation may be beneficial when considering tasks involving absolute work and power. RLC phosphorylation shifts the force-pCa curve to the left. This allows more work to be done and greater power performance, as well as allowing for greater tetanic forces during fast shortening velocities at contraction frequencies eliciting less than maximum contractile force due to higher $+df/dt$ (1; 13; 40). PTP has also been shown to increase the velocity of peak power at 80 Hz in mouse EDL, but not at faster stimulation frequencies (1).

The benefits of potentiation can be seen at low frequency activation of motor units (91). This includes endurance activities consisting of low force repetitions for extended periods of time (91). Due to the requirements of previous contractile activity, examination of potentiation can be confounded by fatigue following muscle activation (80). However, it is this scenario that may provide the greatest benefit of potentiation; the ability to counteract the effects of low frequency fatigue (LFF). LFF is characterized by

reduced Ca^{2+} release from SR due to impairments to excitation contraction coupling at low frequencies following repeated stimulation (30; 46; 113). LFF is considered a more physiological form of fatigue than high frequency fatigue as stimulation frequencies beyond 50 Hz are rarely seen in voluntary activity (reviewed in (52)). Potentiation and fatigue coexist in humans and animals (32; 55; 110). Fowles and Green have shown that potentiation can compensate for LFF in humans in vivo by maintaining twitch force through a prolonged series of isometric leg extensions at 30% maximum voluntary contraction (MVC) (32). It has also been shown that PTP can compensate for LFF in animal models (109). By shifting the force-pCa (-log [Ca2+])curve left, the $[Ca^{2+}]_c$ requirements to meet any given level of force are reduced, allowing for contraction intensity to be maintained, despite reductions in Ca^{2+} release induced by LFF (70; 85; 91).

V. Muscular Dystrophy in Mice:

The *mdx* mouse is a commonly used model of DMD. DMD is a degenerative muscle condition seen in 1 in 3500 live male human births, and very few females (54). The *mdx* line was discovered in a colony of C57BL/10 mice while screening the colony for red blood cell defects when elevated serum pyruvate kinase levels were found (14). It was discovered that both the *mdx* and DMD conditions lack the structural protein, dystrophin, due to X-chromosome linked mutations in the dystrophin gene (14). In the *mdx* mouse, this mutation is a single base substitution in the dystrophin gene resulting in early termination of the protein (94), whereas there are several different mutations seen in DMD, many of them spontaneous new mutations (54).

VI. Dystrophin:

Dystrophin is a peripheral membrane protein. It is associated with several proteins including α and β-dystroglycan, α, β, γ and δ-sarcoglycan and cytoplasmic (syntrophin) subcomplexes (figure 2.2). Laminin-2 (also known as merosin) is a basal lamina protein associated with α-dystroglycan in the extracellular matrix. β-dystroglycan is a transmembrane protein that binds α-dystroglycan and dystrophin. The four sarcoglycan proteins associate to form a transmembrane complex that links to β-dystroglycan through δ-sarcoglycan. The COOH terminus of dystrophin is linked to syntrophin and dystrobrevin, which may play a role in cell signaling as a scaffold or in the formation of synapses (3). The NH_2 terminus of dystrophin is bound to F-actin (111).

Muscle contraction generates force in two directions: longitudinally and radially. Longitudinal forces, resulting from the power-stroke phase of contraction, are transmitted to the bone via the tendon. Radial forces also result from crossbridge formation and the compression of myofilament lattice (17; 99). Since myofilaments are anchored to the sarcolemma, these radial forces are obliged to exert force on the sarcolemma (78; 99). Dystrophin helps stabilize the membrane by distributing the mechanical forces over a wider area of the membrane, and transmitting forces across the sarcolemma via glycoproteins to laminin and the extracellular matrix (31; 50; 78).

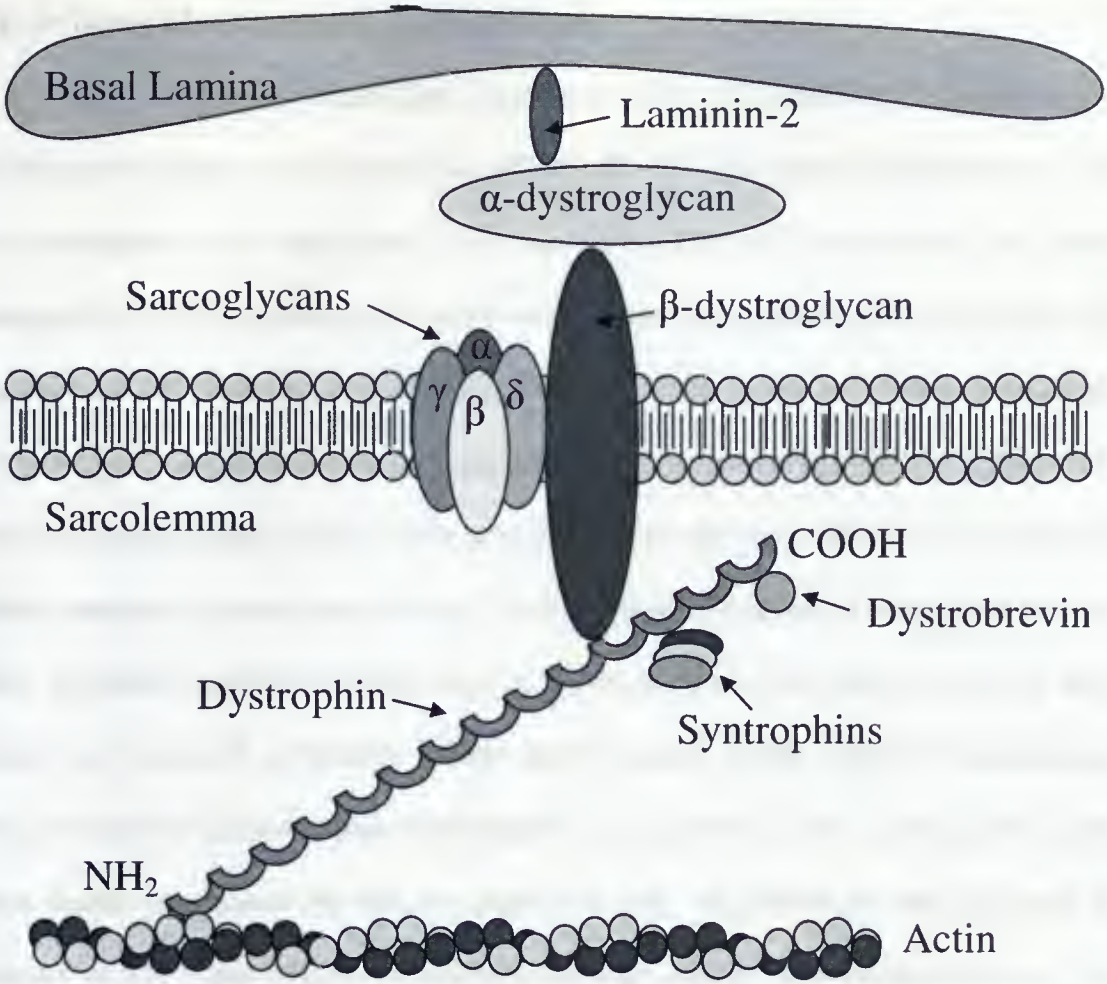

Figure 2.2: Based on Watchko *et al.* (111). Schematic diagram of the dystrophin membrane cytoskeleton in muscle fibers. The protein α-dystroglycan associates with the basal laminar protein laminin-2 and the transmembrane protein β-dystroglycan. A single transmembrane complex is formed by the association of α, β, γ and δ-sarcoglycan. A link is formed between δ-sarcoglycan and β-dystroglycan. On the cytosolic side of the membrane, β-dystroglycan is bound to dystrophin. The NH_2 terminus of dystrophin binds tightly to F-actin, linking it to the sarcolemma and the extracellular matrix. The COOH terminus of dystrophin binds to syntrophin and dystrobrevin (111).

VII. Primary Muscular Dystrophy Attributes:

The sarcolemma in dystrophic muscle is easily wounded due to the absence of dystrophin's effect of force dispersion (20; 31; 50; 78). The greater susceptibility of the *mdx* membrane to wound creates more opportunity for Ca^{2+} influx at rest and during contraction (20; 78). Dystrophic muscle is commonly associated with chronically high intracellular Ca^{2+} concentrations (48; 63; 106). In addition to the influx from wounds, the elevated Ca^{2+} concentration can be attributed to a greater probability of sarcolemmal calcium channels being open in adult muscle fibers of *mdx* mice (48; 63). The activity of these channels is not regulated directly by dystrophin, but rather by proteolytic activity. *Mdx* myotubes cultured in the presence of leupeptin, a protease inhibitor, do not show either the increased probability of the leak channels being open or the increased intracellular $[Ca^{2+}]_c$ that is seen in untreated *mdx* myotubes (105). Elevated $[Ca^{2+}]_c$ has been shown to increase the rate of proteolysis (48; 106) which in turn increases the activity of Ca^{2+} leak channels (105) and reduced activity of sarco/endoplasmic Ca^{2+} ATPase (SERCA) (90). It is the increased susceptibility to wounds in the sarcolemma that ultimately causes necrosis. Although membrane wounds do not necessarily lead to immediate cell death, as the membrane can quickly reseal (20), even a small Ca^{2+} influx will have a large transient increase in the concentration of Ca^{2+} at the wound site. Some proteases, such as μ-calpain, are activated by sarcolemma bound proteins when $[Ca^{2+}]_c$ is elevated (63; 69; 71). Proteases can remain activated long after $[Ca^{2+}]_c$ is no longer sufficient to promote further activation (105). This elevated protease activity affects the leak channels and SERCA, beginning a slow cascade of events leading to the death of the fiber.

The death of a fiber has been found to be caused by both necrotic and apoptotic mechanisms. It has been shown that muscles of mdx mice show apoptotic indicators as young as 2 weeks of age, prior to any evidence of cell necrosis (103). This leads to an increased presence of cytotoxic T-lymphocytes in the muscle and surrounding connective tissue, which have an important role in both mechanisms of cell death (95; 119). CD8+ cytotoxic T-lymphocytes deficient mdx mice showed almost no apoptotic cells, and a 60% reduction in necrotic cells (95).

VIII: Secondary Muscular Dystrophy Attributes:

In *mdx* mice, muscle fibers appear normal up to 10-18 days after birth (28; 53). From 3-4 weeks after birth, muscle fibers in *mdx* mice undergo massive degeneration. In *mdx* mice as young as 3-6 weeks old, fibers exhibit extensive damage compared to control mice. Isolated EDL fibers have been shown to have necrotic regions, centrally located nuclei, membrane lesions and supercontracted areas along the length of the fiber (44; 115) which are indicative of sarcolemmal damage. Damaged fibers activate satellite cells, starting a period of regeneration where nearly all fibers are either repaired or replaced (53). The presence of undifferentiated embryonic fibers was noted in diaphragms of 3-4 month old *mdx* mice but not in 24 month old *mdx* mice or control mice of either age (79). Embryonic fibers may produce lower forces than mature, differentiated fibers (21; 79). In normal mouse and human muscle, embryonic myosin isoforms differentiate by the first week after birth and do not reappear without muscle regeneration (67; 112; 114). Regenerating and repaired muscle fibers first expresses the embryonic myosin isoform, followed by the neonatal isoform, and finally adult myosin isoforms (28;

67; 114). The transition from the embryonic to adult myosin isoforms takes place over a period of 3-4 weeks (67). 10 weeks after birth, only 10% of *mdx* fibers still contain embryonic and neonatal isoforms (28). The regenerative period does not last for the lifetime of the animal, as *mdx* diaphragm fibers have been shown to stop expressing embryonic myosin isoforms by 6 months of age (21).

In both *mdx* mice and humans, there is often marked hypertrophy early in the disease process (100). This initially represents true hypertrophy but the large muscles are weak, representing a contribution of degenerating and necrotic fibers to the CSA. This later becomes pseudohypertrophy as degenerated muscle tissue is replaced first by connective tissue and later by fat (60; 61; 97; 100). From 2-4 weeks of age, *mdx* mice are significantly heavier than control mice (116). Control mice increase in body mass until ~17 months before beginning to lose mass, losing 33% of their peak mass by the time they reach 28 months of age (60). In contrast, *mdx* mice reach peak body mass at ~6 months of age, and lose 25% of this mass by 28 months (60). *Mdx* mice have 30% less mass at 17-24 months compared to control mice, but do not differ from control body mass at 6 and 28 months (60). EDL and soleus muscle masses declined from 6 months to 28 months in both *mdx* and control mice (60). Despite having smaller body masses, *mdx* hind limb muscles are larger than control muscles (60; 89) at all ages (60), with the greatest difference seen at 6 months of age with 28% larger EDL and 42% larger soleus muscles (60). The tibialis anterior has been reported to have 80% larger mass in *mdx* mice (89).

Microscopy studies of adult *mdx* skeletal muscles shows the presence of centrally located nuclei, whereas control muscles have peripherally located nuclei arranged in a

helix along the fiber length (60; 115). Centrally positioned nuclei are used as an indication that a fiber has been replaced or repaired (28; 42; 53) as there is little evidence that nuclei are able to migrate to the periphery (15; 28). The presence of centrally located nuclei is linked to the age of the fiber and the disease progression as *mdx* mice aged 3-6 weeks have centrally located nuclei in 20-30% of fibers, but by 8 weeks 60-90% of *mdx* muscle fibers in adult *mdx* mice are centronucleated, depending on fiber type (23; 28; 53; 59; 60; 115).

Mdx mice show great variation in the cross-sectional area (CSA) of individual fibers, with evidence of extremely large fibers and small atrophic fibers (5; 60; 97). The variability in area is especially evident in type IIA fibers of soleus and in type IIB fibers of EDL (5). While the mean fiber size of *mdx* hind limb muscle is ~25% smaller than in age-matched controls, the total number of fibers in the EDL and soleus are ~35% greater in *mdx* mice (60), which is consistent with the branching of muscle fibers in *mdx* mice (44). Branched fibers are less adept at producing force than unbranched fibers (44). Control mice have a much greater proportion of viable muscle fibers compared to *mdx* mice. Approximately 100% of the CSA in a diaphragm section is composed of viable fibers at any age in control mice, whereas the proportion of the CSA composed of viable fibers in 4-6 month old and 24 month old *mdx* mice is approximately 70% and 40% respectively (61; 79). The remainder is composed of mononuclear cells, degenerating cells, connective tissue and fat (5; 6; 60; 61; 97).

The repair process in *mdx* mice is altered compared to normal mice such that it results in a greater percentage of deformed fibers. There are many fibers that split into two, three or more branches (44; 115) orientated along the longitudinal axis of the muscle

(44). These branches exhibit cytoplasmic continuity and will occasionally rejoin the main body of the fiber (44). While up to 90% of fibers may exhibit branching deformities in *mdx* mice at 6 months of age (44), normal mice recovering from EDL transplantation, only 6.6% of the regenerated fibers showed persistent branching deformity 100 days following the operation (9). Interestingly, shorter fibers seem to have a degree of protection over longer fibers as they exhibit less branching and deformities. In one study, after 26 weeks of age, 90% of EDL fibers and 88% of soleus fibers had malformations, however only 31% of flexor digitorum brevis (FDB) fibers were malformed (44). The fibers of the FDB are ~1/20th the length of either soleus or EDL, but the CSA of each individual fiber is similar (44).

Degeneration is greater in the *mdx* diaphragm than in *mdx* hind limb muscles (15; 97). This is exhibited by greater decrements in active tension and maximum velocity of shortening in diaphragm versus hind limb muscle (29). Optimal twitch and tetanic length are shorter in *mdx* diaphragm than control mice (29; 79; 97), but optimal sarcomere length is constant, reflecting a loss in the total number of sarcomeres (97). Muscle regeneration seems able to reach equilibrium with muscle degeneration in *mdx* hind limb muscle, but not in *mdx* diaphragm or in human DMD muscle (5; 28; 29; 48; 61; 79). This leads to progressive muscle wasting in these muscles, despite normal proliferative capacity of myoblasts and more numerous satellite cells. Indeed, DMD is associated with respiratory problems relating to weakness of the diaphragm and decreasing vital capacity as the disease progresses, often leading to respiratory failure (84; 100). Thus *mdx* mouse diaphragm is the most representative model of DMD in humans. The enhanced degeneration of the *mdx* diaphragm relative to other skeletal muscles is thought to be

caused by its comparatively high workload relative to other skeletal muscles, with a respiration rate around 200 breaths per minute (29; 97). When controlling for body size, the work rate of the mouse diaphragm is five times that of human diaphragm (97). However, fibers from *mdx* diaphragm strips show increasing sarcolemmal damage with increasing amounts of mechanical stress, but not with increasing number of repetitions at any given workload (78). This suggests that the primary mechanism of injury in dystrophic muscle appears to be a function of the magnitude of mechanical stress rather than the duration of activation.

Dystrophic muscle is not damaged uniformly. There is a strong effect of fiber type. Coirault *et al.* (21) have found that 6 month old *mdx* mouse diaphragms display a greater proportion of type IIA fibers and fewer type IIX/D fibers compared to age-matched controls, with 60% IIA, 36% IIX/D and 3% type I in *mdx* and 37% IIA, 55% IIX/D and 5% type I in controls (21). These findings are similar to those of Petrof *et al.* (79) who found a greater proportion of IIA fibers and lower proportions of IIX/D fibers in 3-4 month old *mdx* mouse diaphragm. In 22-24 month old mice, there were virtually no IIX/D fibers in *mdx* diaphragm, but 35% of control fibers were IIX/D. *Mdx* mice at 22-24 months had shifted to slow oxidative fibers, accounting for 48% of all fibers compared to 7% for controls. This resembles fiber type changes reported in DMD (112). In soleus muscle studied at 3-4 weeks and 32 weeks, no significant changes were seen in the content of fast oxidative/glycolytic fibers or slow oxidative fibers aside from the expected age-related increase in slow oxidative fibers seen in both *mdx* and control mice (5). At 32 weeks, *mdx* EDL had a significantly higher proportion of fast

oxidative/glycolytic fibers, and a much lower proportion of fast glycolytic fibers than those of age matched controls or 4 week old *mdx* mice. (5).

Another contributing factor to degeneration of dystrophic muscle is the CSA. Increased fiber size results in a greater volume to surface area ratio and greater forces transmitted to the membrane, which translates into more damage. A study by Karpati *et al.* (53) showed a positive correlation (r=0.86) between fiber area and percent centronucleation of muscle fibers in *mdx* plantaris. This same study reported increasing percentages of centronucleation in *mdx* skeletal muscles over a 1 year period. Fiber hypertrophy was seen with age in the soleus, plantaris, quadriceps, biceps and ocular retractor muscles, with the greatest proportion of centronucleated fibers observed in the muscles with the greatest CSA. Also reported was a damage threshold of 20-25 microns in diameter where fibers below this threshold appeared less susceptible to necrosis. There was a virtual sparing of the ocular rotator muscles with average CSA of 200-250 um^2 that was not seen in the ocular retractors with average CSA 500-600 um^2 (53). Type IIX/D (73; 78) and IIB (112) fibers are most severely affected by the lack of dystrophin. This may be attributed to the greater fiber CSA (7; 96), the greater forces that these fibers produce (60), or a combination of the two. Average human muscle fiber CSA is 2-3 times greater than that of mice (72). This may accelerate the damage process and overtake regenerative processes (5). This may explain why dystrophic mice are able to remain functional throughout the lifespan but humans affected with DMD show progressive degeneration with age in spite of regeneration in IIB fibers (112). There appear to be some adaptive mechanisms in place in regenerated tissue leading to smaller CSAs. For one, regenerated muscle cells are observed to be 20% smaller in diameter than non-

centronucleated fibers (53). This smaller size may simply reflect the overall pattern of fiber type changes from IIB to IIA or I, or it may be an inherent property of fibers regenerated from satellite cells. Likewise, it is also possible that branched muscle fibers are less susceptible to damage than the main fiber due to their increased surface area to volume ratio, resulting in lower forces being transmitted to the membrane.

IX. Muscle Mechanics in *mdx* Mice:

i. Isometric Contractile Characteristics:

Absolute twitch force (P_t) in isolated *mdx* muscle is similar to age-matched control animals in both diaphragm and limb muscles (5; 77; 79; 89), however when normalized, the force per CSA is lower in *mdx* mice (5; 29; 79; 89; 97; 98). Studies with young mice have shown twitch contraction kinetics to be similar between *mdx* and control mice (29; 79; 98). Studies with *mdx* diaphragm older than 18 months have slowed contraction and ½ relaxation times (79; 97), which is consistent with the greater proportion of type I fibers seen with age (21; 79). Faster contraction time has been reported in *mdx* mice as well (89), however greater fatigue resistance was reported in this study as well as others (29; 79; 83; 89), supporting the findings that *mdx* muscle is comprised of a greater proportion of slow myosin isoforms (21; 79). The posterior compartment of the lower leg in old *mdx* mice has been shown to have slower contraction times compared to that of controls, however this effect was not seen in younger mice (83). In spite of the shift to slower fiber types, tibialis anterior muscles of *mdx* mice have been shown to have right shifted force-frequency curves compared to age matched controls in response to shorter contraction times leading to less summation of forces (89).

The authors of this study have no suggestions of a possible mechanism behind this change. Diaphragm however, shows a left shift in the force frequency curve in 24 month old *mdx* mice, as would be expected with a shift to slower fiber types (79).

Absolute tetanic force (P_o) produced by *mdx* muscles is similar to that of control muscle (60; 77; 111), however when normalized for CSA, P_o is lower in *mdx* muscle (23; 29; 60; 61; 77; 98; 111). Muscle hypertrophy compensates for the reductions seen in normalized P_o such that the absolute P_o is adequate for the survival of the mouse (60). Reduced normalized forces may be due to a number of causes. One cause is an increasing proportion of necrotic or degenerating fibers contributing to *mdx* muscle CSA. However, there is evidence that the muscle loss as a proportion of the CSA (70% of CSA is viable fibers in young mice, 40% in old mice) (61; 79) is insufficient to explain the tension losses (50% and 13-25% of control in young and old mice respectively) (79; 97). This suggests that the remaining viable fibers have impaired capacity to produce force. Other studies have found that normalized P_o of *mdx* mice does not significantly decrease with age relative to control mice, though the P_o is consistently lower (60; 61), and normalized P_o tends to increase with age in controls and decrease in *mdx* mice (61).

Data investigating mechanisms other than fiber type shifts are quite limited. One study has found 50% fewer crossbridges formed per unit area in sections of 6 month old *mdx* diaphragm (21). These crossbridges also produced 5% less force on average than crossbridges in control diaphragm (21), though this could conceivably include contributions of degenerating fibers. Other causes worthy of investigation include altered E-C coupling and reduced calcium sensitivity of the myosin complex.

ii. Dynamic Contractile Characteristics:

Studies examining the properties of *mdx* muscle during shortening have shown downshifts in the force velocity relationship, reduced maximum power, reduced work output and lower optimum velocity for power development than control mice (21; 23; 29; 60; 61; 98). These dysfunctions can be partially explained by the greater proportion of slower myosin heavy chain isoforms. However, slower myosin ATPase rates are counterintuitive to the faster crossbridge cycling, lower mechanical efficiency and lower rate constant for crossbridge detachment seen in *mdx* diaphragm (21), clearly indicating that there are other mechanisms at work.

Muscle lengthening during contraction causes greater muscle damage than either concentric or isometric contractions (44; 78). Lengthening during tetanic contraction of *mdx* EDL results in irreversible reductions in normalized P_o of 40-60% following activated lengthening protocols (24; 44; 73), but no force reductions are seen in *mdx* soleus, control soleus or control EDL (44; 73). These drops in force have been linked to membrane damage (24; 73; 78). There is mixed evidence of membrane damage in skeletal muscles of *mdx* or control mice after maximal isometric contractions; however the number of damaged fibers is invariably greater in *mdx* muscle and in fast twitch muscle (73; 78). The damage and force reductions seen in *mdx* mouse EDL following eccentric contraction along with the disappearance of IIB fibers as the disease progresses (79) suggest that faster fibers are more susceptible to damage than slower fibers. The forces developed during active lengthening are higher than the forces that can be developed either isometrically or during active shortening. Additionally, the degree of compression to the myofilament lattice is greatest during eccentric contraction (17),

indicating greater radial force which may be more damaging to the membrane than longitudinal forces (78). There does not appear to be any fiber damage resulting from passive lengthening of immature *mdx* skeletal muscles (116).

Mdx muscle exhibits greater passive stiffness than control muscle as young as 8 weeks old (97; 98). This increase is thought to be caused by the increase in the amount of connective tissue seen in response to muscle wasting (60; 61; 97; 100). It is possible that this loss of elasticity may predispose *mdx* muscle to damage during lengthening activation, as the amount of negative work performed during lengthening is increased with increased stiffness (98). This idea is supported by studies examining Bio 14.6 δ-sarcoglycan-deficient hamsters which exhibit greater elasticity in muscle fibers (22), but no decrements in P_o following active lengthening (111). The lack of sarcoglycan would effect force dispersion across the membrane, but would not affect the continuity of the network anchoring of the contractile elements to the extracellular matrix.

X. Muscle Mechanics in Aging Mouse EDL

Absolute P_o and P_t of the EDL increase from the time a mouse is born up to 14 months of age (5; 37; 116). By the time a mouse reaches 20 months of age, the muscle is less capable to produce force as it has been shown that P_t is reduced in these mice when compared to mice aged 3-14 months (12; 37). The impairments in absolute force seen with advanced age can partially be explained by reduced force per CSA. P_o and P_t normalized to both CSA and muscle weight increase as a mouse reaches adulthood (5; 116), with no changes seen in force normalized to CSA between mice aged 3 months and 10 months (12). The maximum force of skinned EDL fibers has been reported to remain

constant between 3-6 month and 17-23 weeks of age when normalized to CSA (115). In mice aged 26 months, P_o normalized to CSA is reduced 20% compared to 10 month old mice (12). Another study shows P_o per CSA reductions of 30% in 20 month old mice compared to 14 month old mice. Aging-related force impairment can also explained by reductions in CSA with age. The CSA of 20 month old EDL fibers has been shown to be reduced by 20% (37). The force-frequency relationship has been shown to be left shifted in 26 month old EDL compared to 3 month old EDL (12). There was a strong trend towards a left-shifted force-frequency curve in 20 month old mice, but this failed to reach significance (37).

1/2RT and TPT of mouse EDL have been shown to decrease as a mouse matures (5) and remain constant throughout adulthood (12; 37). Peak contraction velocity is faster in immature mouse EDL than adult EDL (5), but does not change with aging (12; 37). Post-tetanic potentiation has been shown to increase as a mouse ages from 3 weeks to 32 weeks (5) though the mechanism behind this is unclear.

Changes during maturation of mice can be explained partly by increases in CSA of muscle as the mouse grows to adulthood (5) resulting in greater absolute force. Altered kinetics and force per CSA ratios can be explained by shift in myosin isoforms, as slow fibers are replaced with faster fibers (5) and embryonic myosin isoforms are replaced with adult myosin isoforms (21; 79).

Changes due to aging may be explained by changes in Ca^{2+} cycling, as aged mice have been shown to have fewer ryanodine and dihydropyridine receptors (82), having the effect of reducing Ca^{2+} signal strength (26). They may also be explained by reductions in

the contractile protein density (37). It is unlikely that changes in myosin isoform are significant with aging as twitch kinetics are not altered with age (12; 37).

Chapter 3

I. Objectives:

Since DMD is a muscle wasting condition, exercise may help improve the quality of life of those with the condition. Regular exercise is known to both strengthen weakened muscles and cause a shift towards slow twitch fibers. This would be beneficial to a person with DMD by strengthening existing fibers to compensate for those lost, and fast twitch fibers may be converted to slower myosin isoforms rather than wasting away. Inducing fiber type shifts towards slow fiber types has been suggested previously as a method for intervening in DMD as slow fibers contain A-utrophin which has been shown to stabilize the dystrophin associated protein complex (18; 19). However, the mechanism of injury for dystrophic muscle is caused by high forces that occur with exercise. Since potentiated muscle generates greater forces, avoiding potentiation could reduce risk of muscle damage. It is therefore possible that muscle of *mdx* mice has down-regulated potentiation in order to prevent fiber damage. Any change in degree of potentiation may be of importance when considering an exercise program that will maximize benefits to those with DMD while simultaneously minimizing risks.

The major objective of this thesis was to determine if potentiation is altered in dystrophic EDL of both young and old *mdx* mice compared with age-matched wild type controls. Another major goal of this thesis was to determine if shifts in muscle fiber type or changes in myosin light chain kinase content could explain potential differences in

potentiation with aging and DMD. Fatigue measurements were also made to help explain the functional role of altered force potentiation. Measurements were performed in EDL muscle of mice at ages 50 days, during a period of fiber regeneration after massive fiber damage has taken place in *mdx* mice, and 10 months, corresponding with more advanced degeneration in *mdx* mice.

II. Hypotheses:

It is hypothesized that there will be a higher percentage of type IIB fibers in EDL from control mice than *mdx* mice. This would be in accordance with previous studies (5; 21). This proportion is expected to be lower in old *mdx* mice than young *mdx* mice due to the fast twitch fiber specificity of the disease (5).

It is hypothesized that potentiation will be reduced in *mdx* mice compared to control mice as a means to protect against fiber damage resulting from high forces. Potentiation is expected to be reduced in old *mdx* mice more than young *mdx* mice to correspond with fiber type shifts towards slower fiber types associated with the condition. Old control mice are expected to potentiate more than young control mice in accordance with previous literature (5).

Finally, it is hypothesized that skMLCK content will be reduced in *mdx* mice. Force potentiation is dependent on skMLCK expression (88). Shifts to slower fiber types are associated with reductions in skMLCK activity (49; 65; 74; 75). As such, it is expected that there will be an effect of age on skMLCK within the *mdx* condition as the proportion of type IIB fibers decreases.

Chapter 4

Methods:

I. Mice:

Mice were obtained from the Jackson Laboratory (Bar Harbor, Maine). Four groups of male mice were examined: Young C57BL/10 (YC, n=8), old C57Bl/10 (OC, n=8), young *mdx* (YM, n=8) and old *mdx* (OM, n=7) (table 4.1). Old mice were obtained as retired breeders and aged to 10 months at Brock University. Young mice were obtained at 2 weeks of age and aged to 52 days. One additional *mdx* mouse is aging and will be completed in January, 2008. Measurements of skMLCK content and fiber typing have been completed for only 6 mice from the OM group, as one mouse reached 10 months of age on December 12, 2007. Young mice and old control mice were housed in groups while old *mdx* mice were housed individually to prevent fighting as per instructions of the animal care committee. Mice had free access to standard chow, water and a running wheel. All procedures were approved by the Brock Animal Care and Use Committee (Protocol # 07-02-01).

Table 4.1: Mouse Characteristics

Mouse	Age (Days ± SE)	Mass (g ± SE) §	n
Young C57BL/10 (YC)	52.8 ± 0.4	22.2 ± 0.6	8
Young *mdx* (YM)	51.6 ± 1.8	25.0 ± 1.3 #	8
Old C57BL/10 (OC)	283-312[1]	33.3 ± 1.7	8
Old *mdx* (OM)	301.6 ± 2.5	32.9 ± 0.4	7

[1] Birth dates were available only as a month and year of birth for Old C57BL/10 mice. Data is presented as a range of means.

Significantly larger than YC

§ Main effect of age was significant (Old > Young; $p<0.05$)

II. Muscle Preparation:

Animals were sedated with Euthanol (0.02 mL /g body weight). The EDL was carefully excised from both legs of each mouse with the tendons intact. Sections of white gastrocnemius and soleus were also taken for further analysis. Muscles were kept on ice in a dissecting medium containing (in mM): 136.5 NaCl, 5.0 KCl, 11.9 $NaHCO_3$, 1.8 $CaCl_2$, 0.40 NaH_2PO_4, 0.10 EDTA and 0.50 $MgCl_2$, pH 7.5 (57) until use. Following muscle removal, the animals were euthanized by injection of Euthanol (0.02 mL/g body weight) into the heart followed by cervical dislocation. Tendons of extracted muscles were tied to a fixed platform at the distal end and a force transducer at the proximal end using non-absorbable braided silk (4-0) and suspended vertically and length was adjusted to 10 mN of tension. Muscles were incubated for 30 minutes at 25°C in an oxygenated (95% O_2-5% CO_2) bath containing a physiological salt solution containing (in mM): 121.0 NaCl, 5.0 KCl, 24.0 $NaHCO_3$, 1.8 $CaCl_2$, 0.40 NaH_2PO_4, 5.50 D-Glucose, 0.10 EDTA and 0.50 $MgCl_2$, pH 7.3 (56). Optimal length for twitch force was found by adjusting the resting tension of the muscle and stimulating at supramaximal voltage until maximal force was found. Stimulation was applied using flanking platinum electrodes and a model 701B stimulator from Aurora Scientific Inc (ASI). Contractile data was measured using a model 300H servomotor (Cambridge Technology Inc.) and digitized

using an ASI model 604A analog to digital interface board. Collection was performed at 1000 Hz using Dynamic Muscle Control Data Acquisition software from ASI and National Instruments, and analysis was performed using Dynamic Muscle Control Data Analysis software (ASI and National Instruments)

III. Contractile Procedure:

Peak tetanic force was measured using 150 Hz stimulation for 0.5 seconds. The muscles were left for 20 minutes to allow myosin to dephosphorylate. Following the recovery period, four twitches were recorded using a 1 Hz stimulation rate. The conditioning stimulus was applied at 20 Hz for 10 s. Post-twitches were measured at 5, 10, 15, 20, 30, 45, 60, 75, 90, 120, 180, 240, 300, 360, 420, 600, 1200 and 1800 seconds after the completion of the conditioning stimulus. The muscle was then randomly subjected to either a phosphorylation or a fatigue protocol with each mouse having an EDL assigned to each group.

The phosphorylation group was given four baseline twitches at 1 Hz, and a second conditioning stimulus at 20 Hz for 10 seconds. Post-twitches were measured at 5, 10 and 15 seconds after the cessation of the conditioning stimulus and the muscle was immediately freeze clamped and stored for RLC phosphate content and Western blot analysis.

The fatigue group was given a single twitch followed by a tetanic contraction at 150 Hz for 0.5 s. The muscle was then stimulated at 40 Hz for 60 seconds followed immediately by a post-twitch and a second tetanic contraction. Fatigue was assessed by determining the time (s) in took to reach 50% of initial force. The muscle was then

mounted in embedding medium and frozen in cold isopentane for histochemical analysis. Refer to figure 4.1 for a flowchart outlining the contractile procedure.

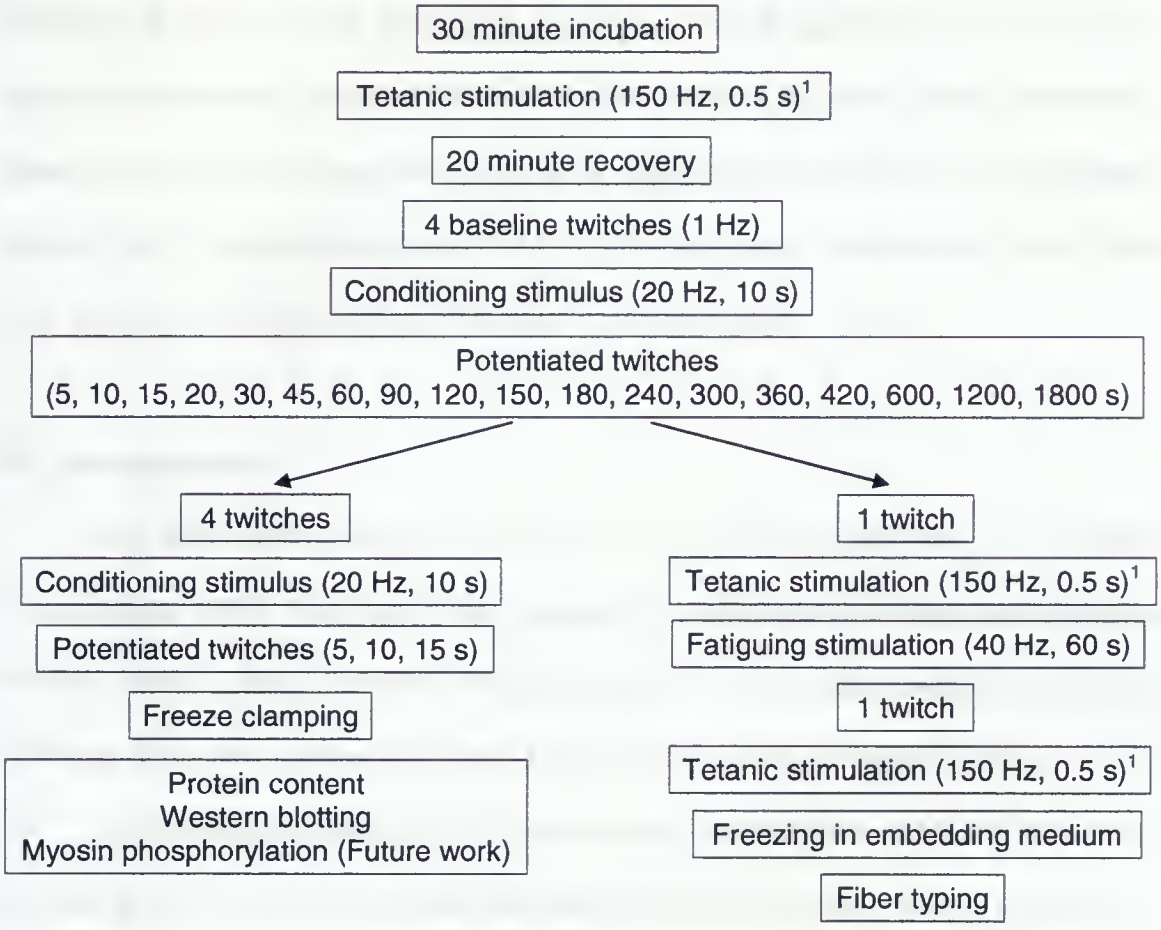

Figure 4.1: Flowchart outlining contractile procedure and biochemical measurements to be taken from each muscle.

[1] Some muscles generated forces in excess of 490 mN which was beyond the range of the force transducer being used. In these muscles a 70 Hz contraction was used rather than 150 Hz

Twitch kinetics measured include half relaxation time (1/2RT), time to peak tension (TPT), rate of force production (*+df/dt)* and rate of relaxation (*-df/dt).* 1/2RT was measured as the time from peak force to the time of half peak force in the relaxation phase of a contraction. TPT was measured from the time of first force development to the time of peak force. The maximal value of the first derivative of the force development phase of the contraction was taken to be *+df/dt.* The value of largest magnitude of the first derivative of the force decay phase was designated *-df/dt.*

IV. Histochemistry:

For fiber type analysis, serial 10 μm cross sections were cut in a cryostat maintained at -20°C. After air drying, sections of muscle were fiber typed using myosin ATPase azure A stain, measuring ATPase activity at pH 9.4 after preincubation at pH 4.60 and 10.30 and classified as Type I, Type IIA, Type IIX/D or Type IIB (76).

Immunohistochemistry was to be performed to determine skMLCK and $PP1_M$ content in fiber types, however the antibodies produced for these proteins exhibit non-specific binding and were deemed unfit for this purpose.

V. Western Blotting:

Western blot analysis was performed in duplicate to analyze skMLCK and $PP1_M$ in whole muscle homogenates. Protein concentrations were determined by the method of Lowry as modified by Schacterle and Pollack (92). Separation was performed using 7.5 μg of total protein loaded into 7.5% polyacrylamide gels using SDS/PAGE. Two mice from each condition were loaded in each gel along with a standard of 7.5 μg total protein

of homogenized mouse EDL. This was followed by transfer to nitrocellulose membranes. Membranes were probed using anti-skMLCK and anti-$PP1_{\beta}$ polyclonal goat antibodies. Primary antibodies were obtained from Santa Cruz Biotech: sc-9456 polyclonal goat IgG (anti-skMLCK) and sc-6106 polyclonal goat IgG (anti-$PP1_{\beta}$). Secondary probing was performed with donkey anti-goat antibody conjugated with horseradish peroxidase. Quantification was performed using an enhanced chemiluminescence detection kit and densitometric analysis. Data is expressed as a percentage of the light density of the standard.

VI. Statistical Analysis:

To determine the effects of age (young vs. old), condition (CTL vs. *mdx*) and time a three-way repeated measures analysis of variance (ANOVA) was employed. A two-way ANOVA was used to determine significance of protein content and fiber type. Post-hoc testing was performed using Tukey's HSD. $P < 0.05$ was considered statistically significant. All data are presented as mean ± standard error (SE).

Chapter 5

Results:

I. Mouse Characteristics:

Age significantly increased the mass of both *mdx* and control mice ($p<0.001$). YM were significantly heavier than YC ($p<0.05$), but no significant differences were found between OC and OM (table 4.1).

II. Force Analysis:

Maximum tetanic force was higher in old mice compared with young mice in both Control and *mdx* groups (figure 5.1, table 5.1). Some mice in the OM and OC conditions produced more force than the 490 mN transducer was able to measure, as such, tetanic force is under reported in this study in the older conditions. The *mdx* mice had lower tetanic force than control mice at both 50 days (280 ± 25 mN versus 320 ± 15 mN) and 10 months of age (390 ± 22 mN versus 421 ± 9 mN).

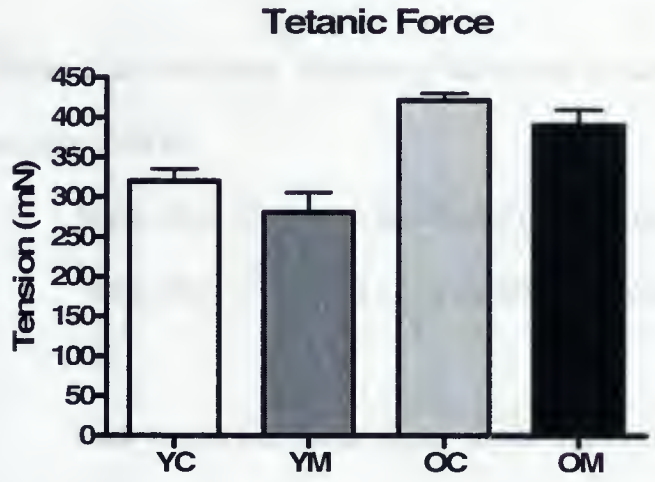

Figure 5.1: Histogram displaying maximum force of EDL muscles stimulated for 0.50 seconds at 150 Hz.

Main effect of age was significant (Old > Young; $p<0.001$)

Main effect of condition was significant (Control > *mdx*; $p<0.05$)

At 40 Hz, old mice produced more forceful contractions than young mice and control mice produced more force than age matched *mdx* mice (figure 5.2).

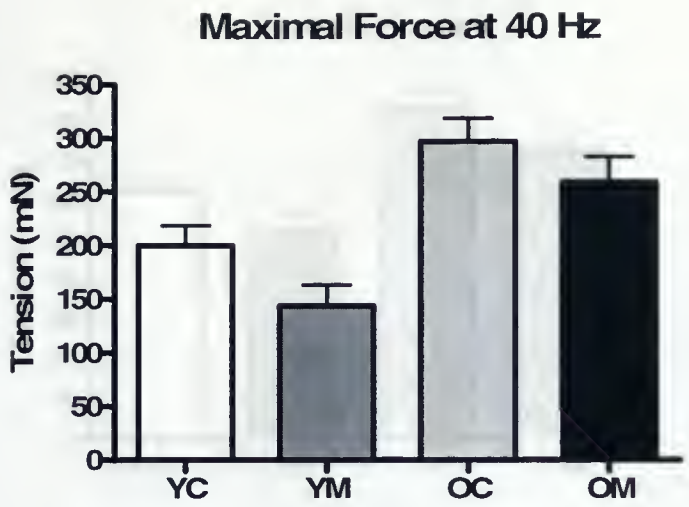

Figure 5.2: Histogram displaying maximum force of EDL muscles stimulated for 60 seconds at 40 Hz.

Main effect of age was significant (Old > Young; $p<0.001$)

Main effect of condition was significant (Control > *mdx*; $p<0.05$)

Peak twitch force was higher in old mice compared with young mice in both the *mdx* and control conditions (figure 5.3). The *mdx* mice had lower twitch force than control mice at both 50 days (52.3 ± 5.1 mN versus 62.5 ± 2.7 mN) and 10 months of age (83.0 ± 5.1 mN versus 73.3 ± 4.6 mN).

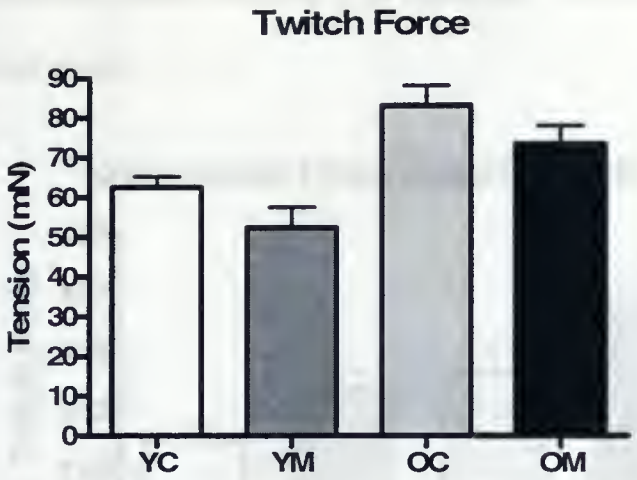

Figure 5.3: Histogram displaying maximum twitch force of EDL muscles.

Main effect of age was significant (Old > Young; $p<0.001$)

Main effect of condition was significant (Control > *mdx*; $p<0.05$)

Maximum potentiation was determined for each muscle at a time corresponding to the maximum tension. This occurred between 10 and 20 seconds after the cessation of the conditioning stimulus for every muscle. When normalized to the force produced under basal conditions, there was a significant interaction whereby the relative potentiation was highest in OM compared with all other groups (figure 5.4, 5.5, table 5.1). However, in general *mdx* mice showed greater potentiation than control mice, and old mice potentiated more than young mice (figure 5.4). Twitch potentiation declined exponentially over the 30 minutes following the end of the conditioning stimulus, returning to near-baseline levels after 10 minutes (figures 5.5, 5.6). The forces did not return to baseline after 10 minutes, and had still not dropped to baseline after 30 min (10 min = 20 min = 30 min > baseline force; $p<0.05$). Potentiation peaked in all conditions 10 seconds after the end of the conditioning stimulus (figure 5.5). After 10 minutes, the

force was close to baseline in all conditions. This suggests that $PP1_M$ activity was similar in all groups.

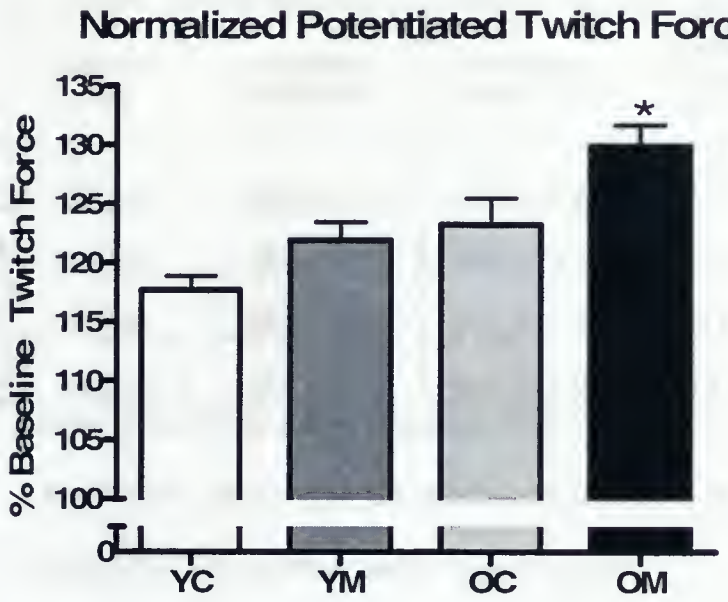

Figure 5.4: Histogram displaying maximum potentiated twitch force of EDL muscles relative to baseline twitch force.

* Significantly higher than OC, YC and YM ($p<0.05$).

Main effect of age was significant (Old > Young; $p<0.001$)

Main effect of condition was significant (*mdx* > Control; $p<0.01$)

Table 5.1: Force for tetanus, baseline twitches, potentiated twitches and normalized potentiated twitches.

	Force - Mean ± SE				
	Tetanus (mN) *	Unpotentiated Twitch (mN) *	Potentiated Twitch (mN) *	Normalized Potentiated Twitch (% Unpotentiated Twitch Force) * ‡	Normalized Twitch 10 Min Post-CS (% Unpotentiated Twitch)
YC	320 ± 15	62.5 ± 2.8	73.4 ± 3.6 §	117.7 +/- 1.2 †	104.3 ± 0.9
YM	280 ± 25	52.3 ± 5.3	66.6 ± 6.3 §	121.9 +/- 1.6 †	103.3 ± 0.9
OC	421 ± 9	83.0 ± 5.2	96.7 ± 5.1 §	123.2 +/- 2.3 †	102.5 ± 1.0
OM	390 ± 22	68.5 ± 6.8	94.2 ± 6.8 §	129.8 +/- 1.9 # †	103.3 ± 0.9

* Main effect of age (Old < young; $p<0.05$)

§ Significantly higher than unpotentiated twitch ($p<0.001$)

‡ Main effect of condition (*mdx* > control, $p<0.05$)

Significantly greater than YC, OC, YM ($p<0.05$)

† Significantly greater than normalized twitch 10 min post-CS ($p<0.001$)

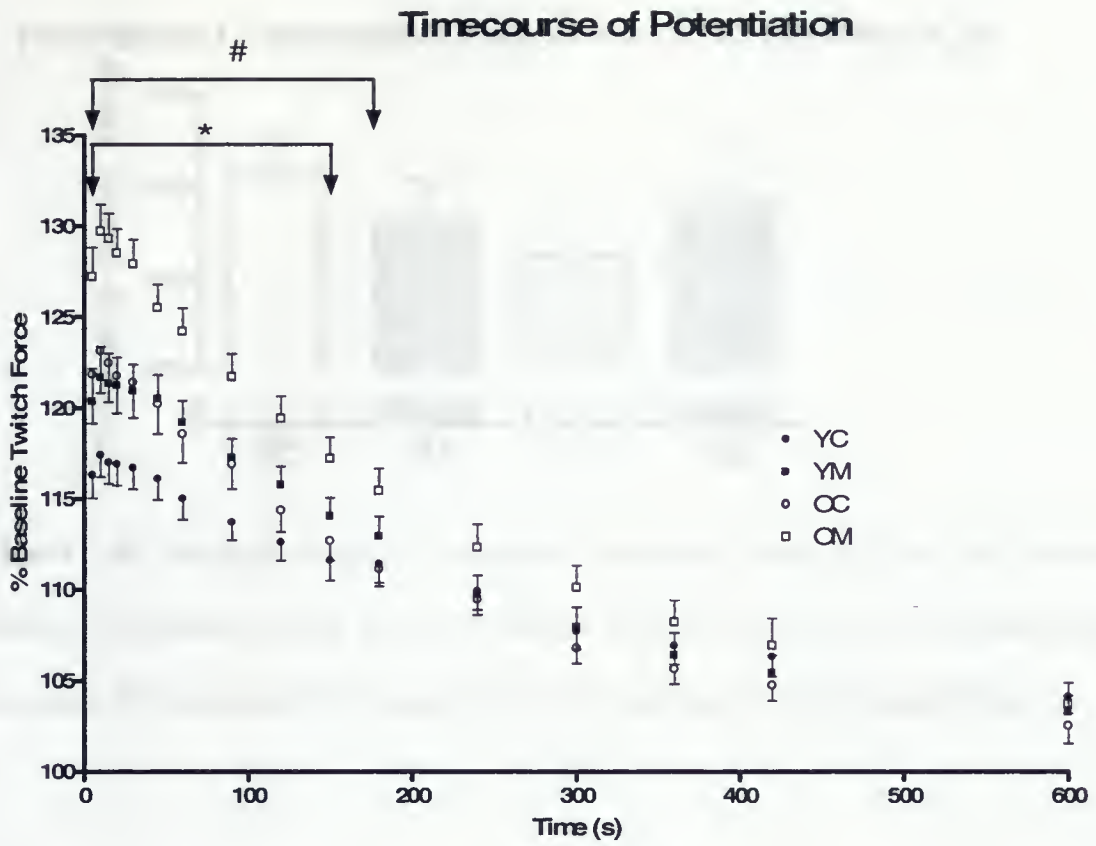

Figure 5.5: Twitch potentiation in the 10 minutes following cessation of the conditioning stimulus in mouse EDL muscle. Error bars represent ± SE.

* *Mdx* significantly greater than control ($p<0.05$)

Old significantly greater than young ($p<0.05$)

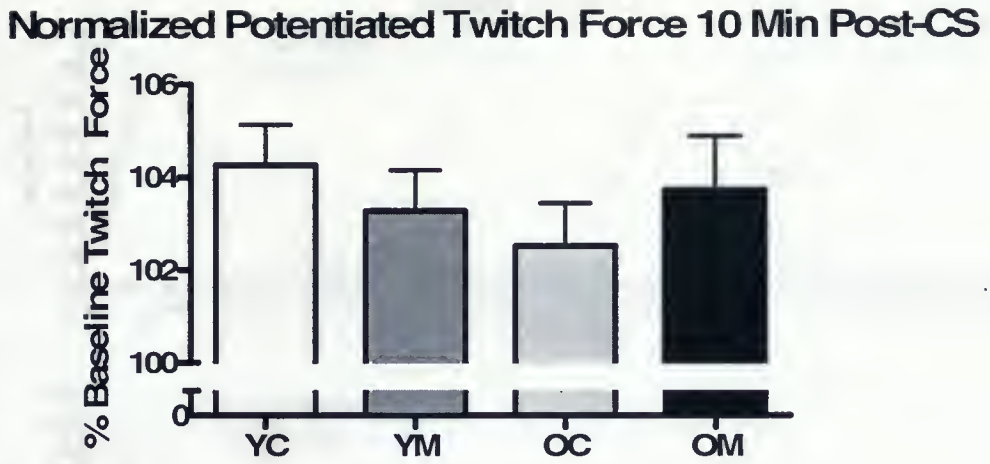

Figure 5.6: Histogram displaying maximum potentiated twitch force of EDL muscles relative to baseline twitch force 10 minutes following the end of the conditioning stimulus. By the end of 10 minutes, force levels were almost back to basal levels.

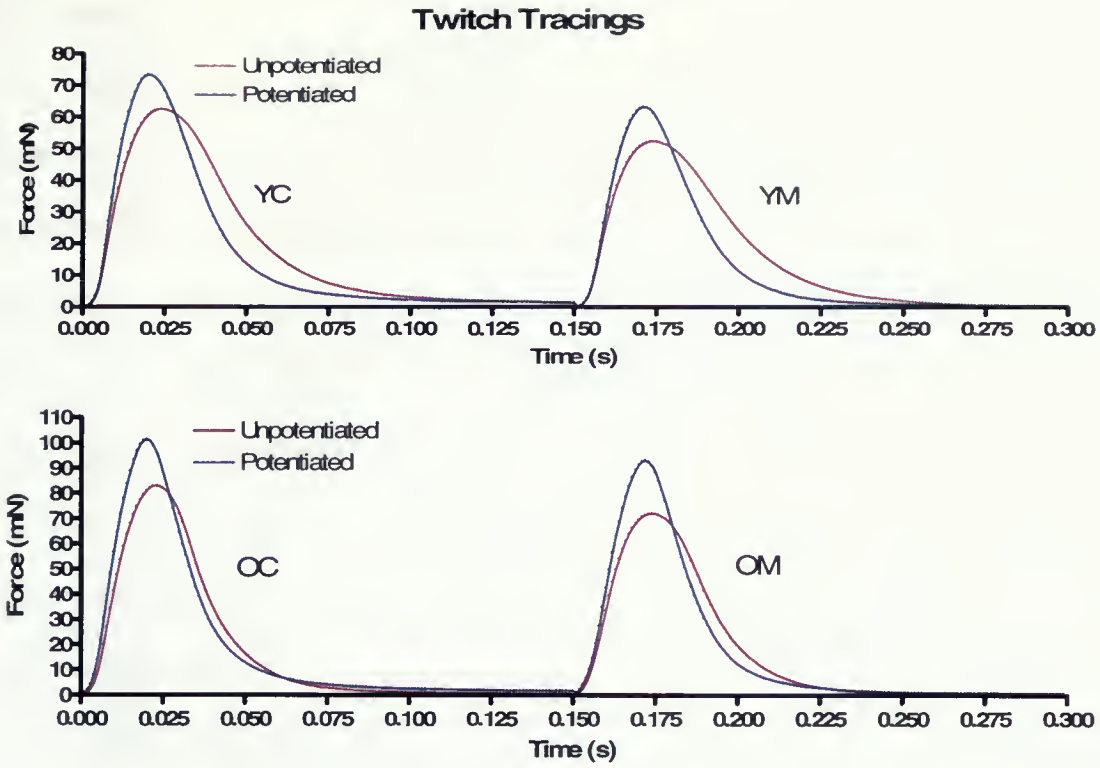

Figure 5.7: Twitch tracings of mouse EDL in both control and potentiated states. Potentiated twitches have faster rates of force production and relaxation, higher absolute force, shorter 1/2RT and shorter time to peak tension (TPT).

III. Kinetic Analysis:

Half relaxation time (1/2RT) of both tetanic and potentiated twitch contractions was not different between conditions; however, 1/2RT of the unpotentiated twitch was longer in young mice compared with old mice (table 5.2). Immediately following the conditioning stimulus, 1/2RT was reduced by 20-30% in all conditions. By 10 minutes following the conditioning stimulus, 1/2RT was ~20% longer than baseline values and remained longer throughout the experiment.

Table 5.2: 1/2RT for tetanus, baseline twitches, potentiated twitches and normalized potentiated twitches.

1/2 Relaxation Time - Mean ± SE					
	Tetanus (ms)	Unpotentiated Twitch (ms) *	Potentiated Twitch (ms)	Normalized Potentiated Twitch (% Unpotentiated Twitch)	Normalized Twitch 10 Min Post-CS (% Unpotentiated Twitch)
YC	28.1 ± 0.8	21.5 ± 0.8	15.9 ± 0.4 §	75.8 ± 2.2 †	121.1 ± 1.8
YM	29.9 ± 1.0	21.4 ± 1.0	15.2 ± 0.5 §	71.8 ± 2.3 †	120.7 ± 2.0
OC	27.1 ± 1.9	18.9 ± 0.9	14.9 ± 0.7 §	79.5 ± 2.5 †	114.8 ± 3.1
OM	29.9 ± 1.9	19.9 ± 0.9	15.2 ± 0.8 §	76.6 ± 2.3 †	120.0 ± 2.7

* Main effect of age (Young > old; $p<0.05$)

§ Significantly shorter than unpotentiated twitch ($p<0.01$)

† Significantly less than normalized twitch 10 min post-CS ($p<0.001$)

The results for time to peak tension (TPT) are shown in table 5.3. Potentiated twitches in older mice took longer to reach peak tension than in younger mice. Young *mdx* mice had significantly lower TPT in baseline twitches than other groups (YM: 23.5 ± 0.3 ms versus YC: 24.4 ± 0.4 ms, OC: 24.7 ± 0.5 ms, OM: 25.1 ± 0.6 ms).

Table 5.3: TPT for baseline twitches, potentiated twitches and normalized potentiated twitches.

Time to Peak Tension - Mean ± SE				
	Unpotentiated Twitch (ms)	Potentiated Twitch (ms) *	Normalized Potentiated Twitch (% Unpotentiated Twitch) *	Normalized Twitch 10 Min Post-CS (% Unpotentiated Twitch)
YC	24.4 ± 0.4	20.6 ± 0.3 ‡	86.4 ± 1.6 †	102.4 ± 1.4
YM	23.5 ± 0.3 §	20.4 ± 0.4 ‡	87.1 ± 1.5 †	99.7 ± 2.1
OC	24.7 ± 0.5	22.2 ± 0.4 ‡	90.4 ± 1.7 †	100.9 ± 1.7
OM	25.1 ± 0.6	22.7 ± 0.6 ‡	90.9 ± 1.9 †	103.3 ± 2.8

Main effect of *mdx* (Control > *mdx*; $p<0.05$)

* Main effect of age (Old > young; $p<0.05$)

§ Significantly shorter than YC, OC and OM ($p<0.05$)

† Significantly less than normalized twitch 10 min post-CS ($p<0.01$)

‡ Significantly shorter than unpotentiated twitch ($p<0.01$)

The *mdx* condition showed a strong trend towards lower peak rates of force development (+*df/dt*) in both potentiated (p=0.081) and unpotentiated twitches (p=0.079), but this did not reach statistical significance and the effect disappeared when the +*df/dt* of the potentiated twitch was normalized to the +*df/dt* of the unpotentiated twitch (table 5.4). There was a main effect of age ($p<0.05$) during tetanus, unpotentiated twitches and potentiated twitches.

Table 5.4: +*df/dt* for tetanus, baseline twitches, potentiated twitches and normalized potentiated twitches.

+*df/dt* - Mean ± SE

	Tetanus (mN/s) *	Unpotentiated Twitch (mN/s) *	Potentiated Twitch (mN/s) *	Normalized Potentiated Twitch (% Unpotentiated Twitch)	Normalized Twitch 10 Min Post-CS (% Unpotentiated Twitch)
YC	5590 ± 310	5870 ± 240	7290 ± 290 ‡	124.1 ± 1.4 †	104.3 ± 1.0
YM	5300 ± 490	5050 ± 510	6250 ± 620 ‡	124.6 ± 1.1 †	106.2 ± 0.9
OC	6860 ± 370	7170 ± 450	8850 ± 570 ‡	123.3 ± 1.2 †	106.1 ± 0.9
OM	6880 ± 380	6500 ± 440	8050 ± 520 ‡	124.2 ± 0.9 †	105.7 ± 0.6

* Main effect of age (Old > Young; $p<0.05$)

† Significantly greater than normalized twitch 10 min post-CS ($p<0.001$)

‡ Significantly greater than unpotentiated twitch ($p<0.001$)

Results for maximal rates of relaxation (*-df/dt*) are shown in table 5.5. Tetanic *-df/dt* was significantly faster in OC compared with YC (-22007 ± 810 mN/s versus -17253 ± 993 mN/s). Older mice had faster relaxation rates than younger mice in both baseline and potentiated twitches. When normalized to baseline twitches, potentiated twitches of *mdx* mice had greater increases in relaxation rates than control mice with increases of 31 and 30% for young and old control mice and 48 and 40% in young and old *mdx* mice. Relaxation rates decreased to ~85% of baseline values 10 minutes after the conditioning stimulus and remained depressed for the duration of the experiments.

Table 5.5: *-df/dt* for tetanus, baseline twitches, potentiated twitches and normalized potentiated twitches.

-df/dt - Mean ± SE					
	Tetanus (mN/s) *	Unpotentiated Twitch (mN/s) *	Potentiated Twitch (mN/s) *	Normalized Potentiated Twitch (% Unpotentiated Twitch) #	Normalized Twitch 10 Min Post-CS (% Unpotentiated Twitch)
YC	-17300 ± 1000	-2330 ± 130	-3020 ± 150 ‡	131.1 ± 5.5 †	85.6 ± 2.5
YM	-14800 ± 1600	-2050 ± 260	-2730 ± 240 ‡	147.7 ± 8.9 †	84.1 ± 1.8
OC	-22000 ± 1000 §	-3580 ± 290	-4510 ± 270 ‡	130.4 ± 5.3 †	86.7 ± 3.2
OM	-18100 ± 1500	-3020 ± 220	-4140 ± 280 ‡	140.3 ± 6.7 †	85.4 ± 3.6

Main effect of *mdx* (*mdx* > Control; $p<0.05$)

* Main effect of age (Old > Young; $p<0.05$)

§ Significantly greater than YC ($p<0.05$).

† Significantly greater than normalized twitch 10 min post-CS ($p<0.001$)

‡ Significantly greater than unpotentiated twitch ($p<0.01$)

In the second bout of potentiation, baseline twitches increased in all conditions. Normalized potentiation was depressed in all conditions as well; however, absolute potentiated twitch force was not different between the two bouts (table 5.6). These findings can most likely be explained by Ca^{2+} uptake impairment as suggested by depressed 1/2RT and *-df/dt* after the first bout of PTP.

Table 5.6: Force and potentiation in the first and second rounds of PTP measurement.

	Force - Mean ± SE					
	Unpotentiated PTP Bout 1 Twitch (mN) * §	Unpotentiated PTP Bout 2 Twitch (mN) * §	Normalized Potentiated PTP Bout 1 Twitch (% Unpotentiated Twitch) #	Normalized Potentiated PTP Bout 2 Twitch (% Unpotentiated Twitch) #	Potentiated PTP Bout 1 Twitch (mN) §	Potentiated PTP Bout 2 Twitch (mN) §
YC	65.3 ± 3.1	66.6 ± 2.9	114.0 ± 2.9	113.3 ± 1.9	74.3 ± 3.6	75.5 ± 3.6
YM	59.5 ± 7.0	62.0 ± 7.6	121.5 ± 3.0	119.6 ± 7.1	71.5 ± 7.7	71.6 ± 7.1
OC	85.1 ± 7.9	89.0 ± 7.7	124.6 ± 3.4	118.7 ± 2.6	104.9 ± 8.0	104.9 ± 7.9
OM	69.1 ± 9.7	74.4 ± 10.6	129.6 ± 3.8	123.7 ± 3.7	88.4 ± 10.7	90.1 ± 10.4

Main effect of bout 1 versus bout 2 was significant (Pre > Post, $p<0.001$)

* Main effect of bout 1 versus bout 2 was significant (Post > Pre, $p<0.001$)

§ Main effect of age was significant (Old > Young, $p<0.05$)

IV. Fatigue Characteristics:

YM was more fatigue resistant than all other groups as indicated by the longer time required for force to drop to 50% of initial force (YM, 13.8 ±1.1 s vs. OM, 10.2 ± 0.9 s vs. YC, 10.9 s ± 0.4 s vs. OC, 11.4 ± 0.8 s) (figures 5.8, 5.9).

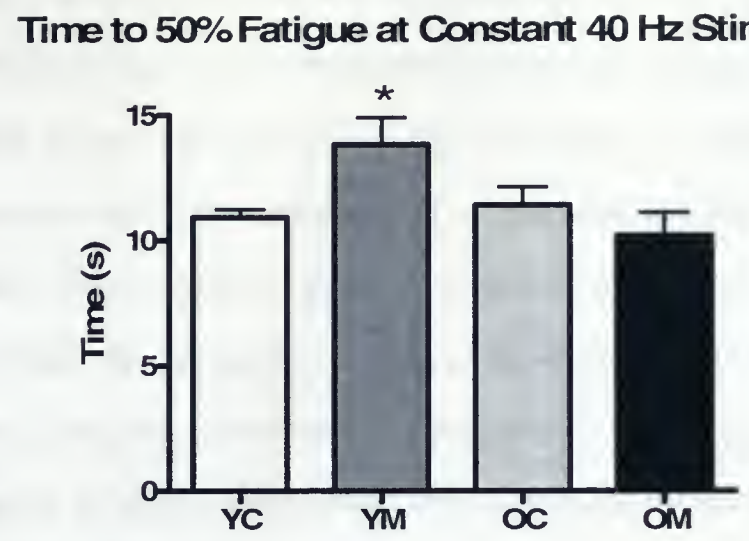

Figure 5.8: Histogram of time to 50% fatigue at constant 40 Hz stimulation.

* Significantly higher than OM ($p<0.01$) and YC ($p<0.05$).

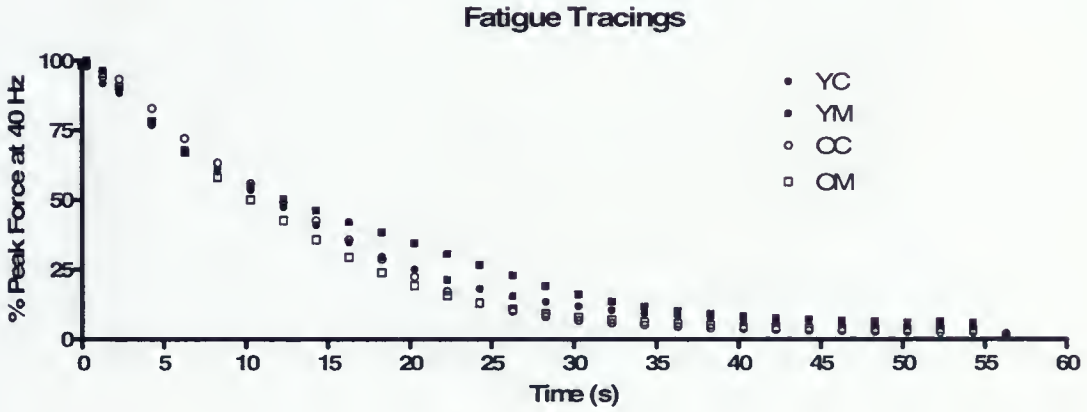

Figure 5.9: Tracings of fatiguing EDL muscle at 40 Hz stimulation.

V. Fiber Typing and Histochemistry:

Representative cross sections are shown in figures 5.10-5.12 and mean results are summarized in figure 5.13. The content of type I fibers dropped from 2.5 ± 0.7% (YC)

and 2.2 ± 0.6% (YM) to 0.4 ± 0.2% (OC) and 1.7 ± 0.4% (OM). The proportion of type IIB fibers was lower in OM muscle (29 ± 3.1%) than other conditions (YC, 39.9 ± 2.3%, YM, 39.9 ± 2.1%, OC, 38.0 ± 3.5%). The proportion of IIX/D fibers was higher in OM muscle at 69 ± 2.6% compared to 61 ± 3.2 % in OC and 58 ± 1.8 % in YM and 58 ± 1.8% in YC. Histochemical analysis also showed the presence of centronucleated cells as well as large necrotic regions in *mdx* muscle, whereas in YC and OC nuclei were located along the periphery and there was no large scale necrosis (figure 5.12). It appeared that a greater proportion of OM fibers were centronucleated than those of YM, however, this data was not analyzed.

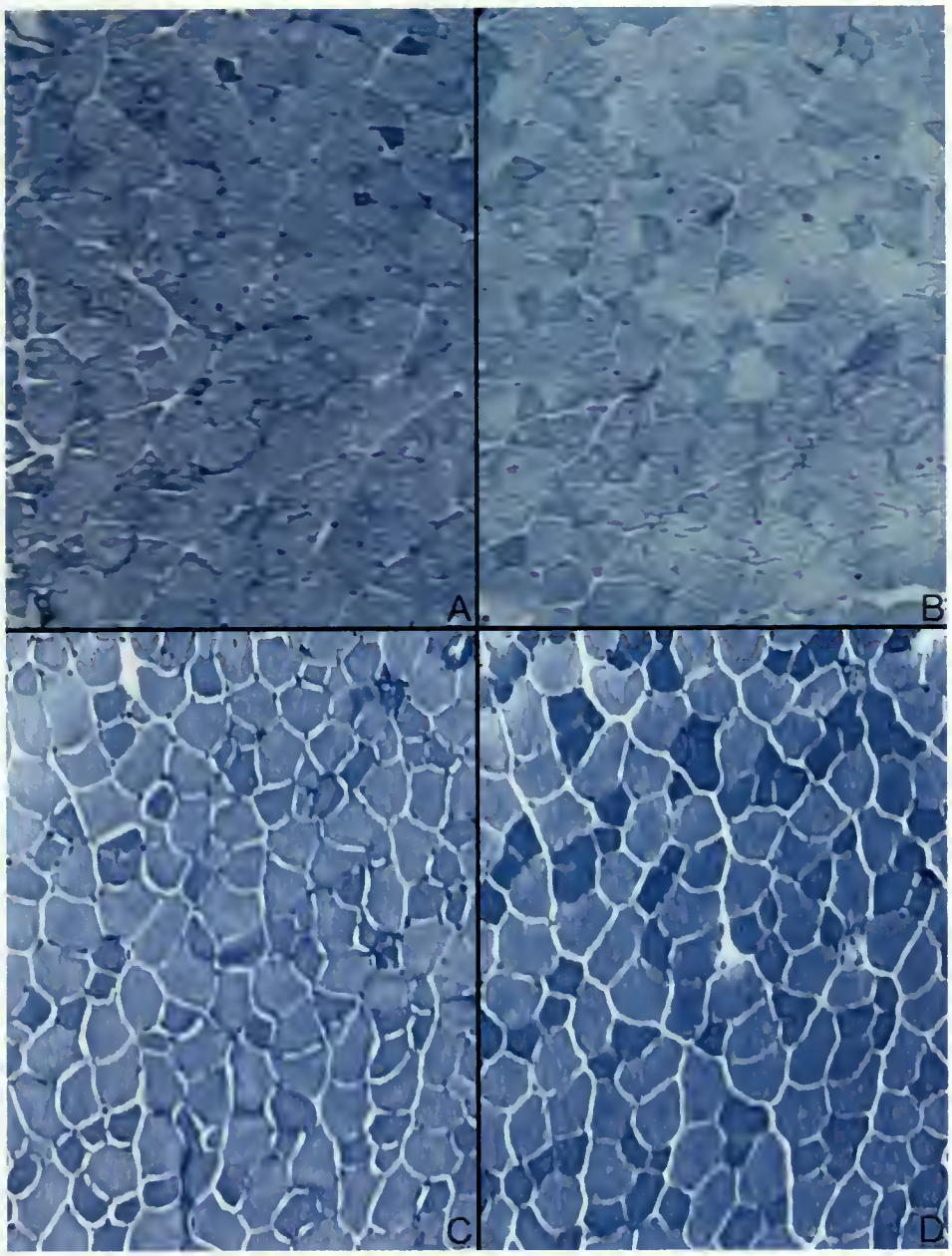

Figure 5.10: Histochemistry of control muscle. Panel A: Young, pH 4.55 Panel B: Young, pH 10.3 Panel C: Old, pH 4.55 Panel D: Old pH 10.3

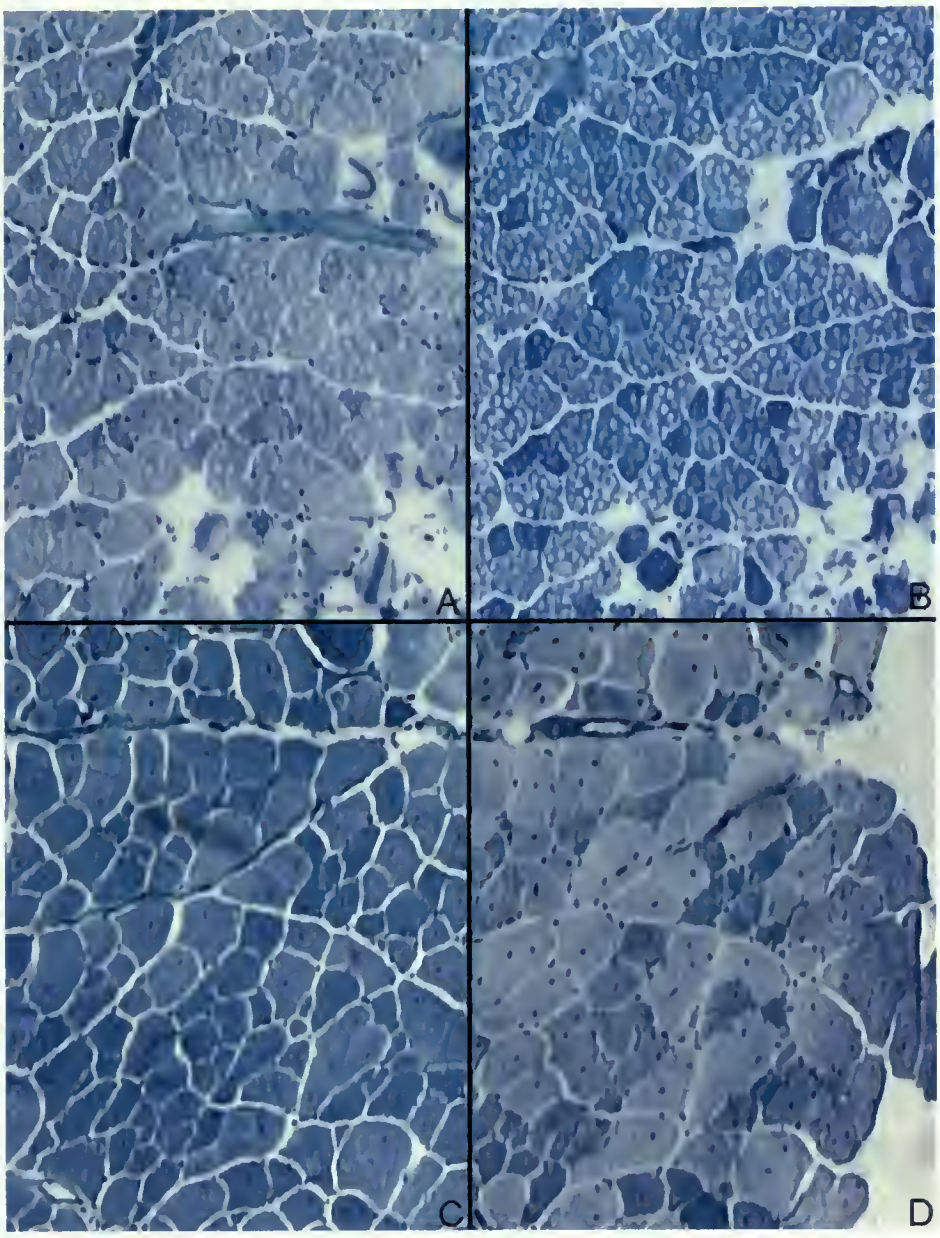

Figure 5.11: Histochemistry of *mdx* muscle Panel A: Young, pH 4.55 Panel B Young, pH 10.3 Panel C: Old, pH 4.55 Panel D: Old, pH 10.3 Note the high degree of centronucleation.

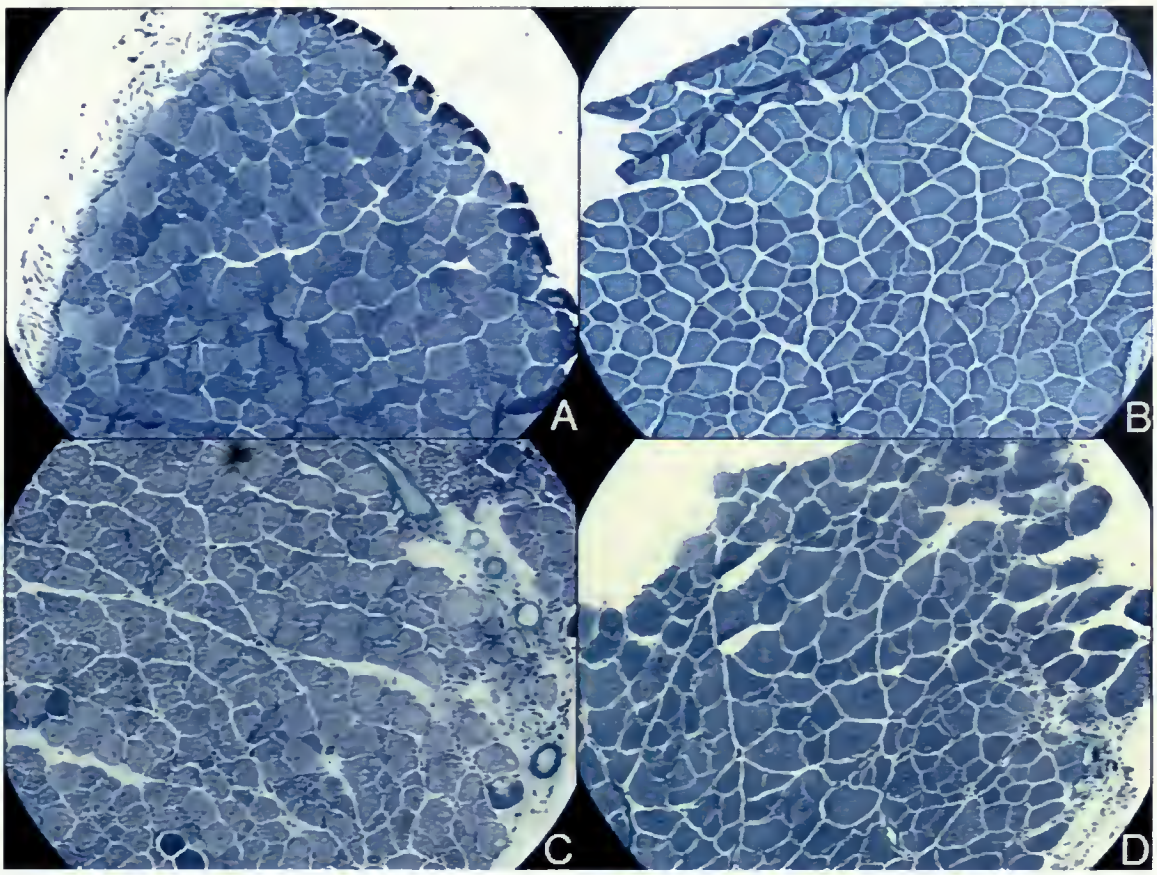

Figure 5.12: Cross sections of mouse EDL muscle showing ATPase activity following pre-incubation at pH 4.55, incubation at pH 9.4 with ATP and staining with Azure A. Panel A: YC, Panel B: OC, Panel C: YM, Panel D: OM. Note the large necrotic regions and centronucleation in panels C and D. In panel D there is also a noticeably larger variation in fiber size.

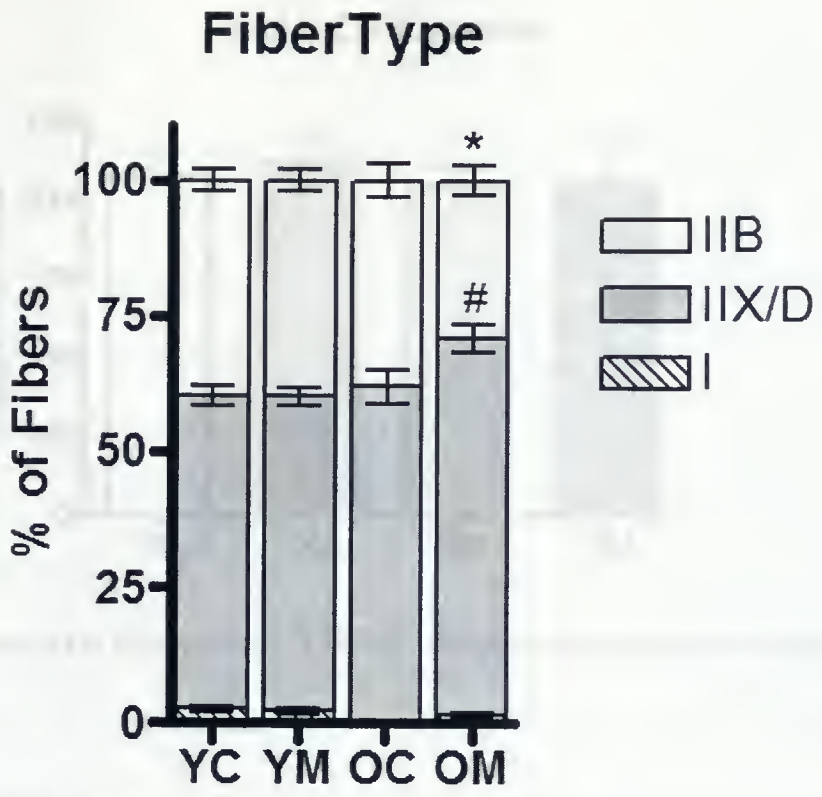

Figure 5.13: Histogram of fiber type proportions present in EDL muscle.

Significant main effect of age in proportion of type I fibers (Young > old, $p<0.05$)

* Significantly fewer IIB fibers proportionately than YC, YM, OC ($p<0.05$)

Significantly more IIX/D fibers proportionately than YC, YM, OC ($p<0.05$)

VI. skMLCK and $PP1_{\beta}$ Content:

There were no significant differences seen in skMLCK (79 kDa) content between any conditions (figures 5.14, 5.15). $PP1_{\beta}$ antibody proved to be too non-specific to provide any usable results for the purposes of this study (data not shown).

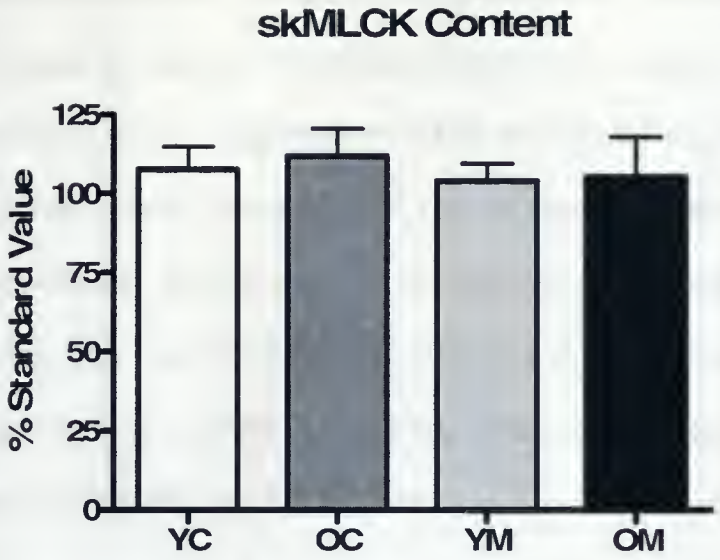

Figure 5.14: Histogram of skMLCK content in homogenized mouse EDL.

Figure 5.15: Representative Western blot of skMLCK protein content. The standard in the second well from the left is a sample of 7.5 µg total protein of homogenized mouse EDL kept constant over all gels. Samples from two mice of each condition were loaded into each gel and each gel was run in duplicate.

Chapter 6

Discussion:

The findings of this study are contradictory to the hypothesized results. Force potentiation in EDL of *mdx* muscle is not down-regulated relative to control mice as a

method to minimize damage. Instead, potentiation is up-regulated in the *mdx* condition at both ages studied. The mechanism by which potentiation is up-regulated is unclear from the results of this study. Since both OM and YM exhibited higher potentiation than aged matched controls, fiber type shifts can not explain the up-regulation. Only OM differed from controls, and this shift was towards a greater proportion of IIX/D fibers, which are slower than type IIB fibers (68; 86). This shift is counterintuitive to what would be expected from a slower muscle fiber as slower fibers tend to potentiate less than faster muscle fibers (65; 74; 75) as the primary role of potentiation is to maintain force levels during prolonged low level stimulation in order to counteract fatigue (32; 80; 85).

The fiber type shift towards slower fibers in OM is consistent with previous research (5; 21; 79). The staining of cross sections suggested a transition from IIB to IIX/D fibers rather than IIB to IIA, as the myosin ATPase did not seem to be fully deactivated in any cells at pH 4.55 as would be expected if there were IIA fibers present. Comparison of EDL cross sections to soleus cross sections supports this finding (figure 6.1). This is also supported by an analysis of EDL of C57BL/6 mice using high resolution electrophoresis. This study reported that there is a very small proportion of IIA myosin present at 50 days and none beyond 90 days (2). Immunohistochemistry of muscle cross sections in the present study would provide a clearer and more accurate description of the fiber types than pH incubations, as well as allow identification of hybrid fibers.

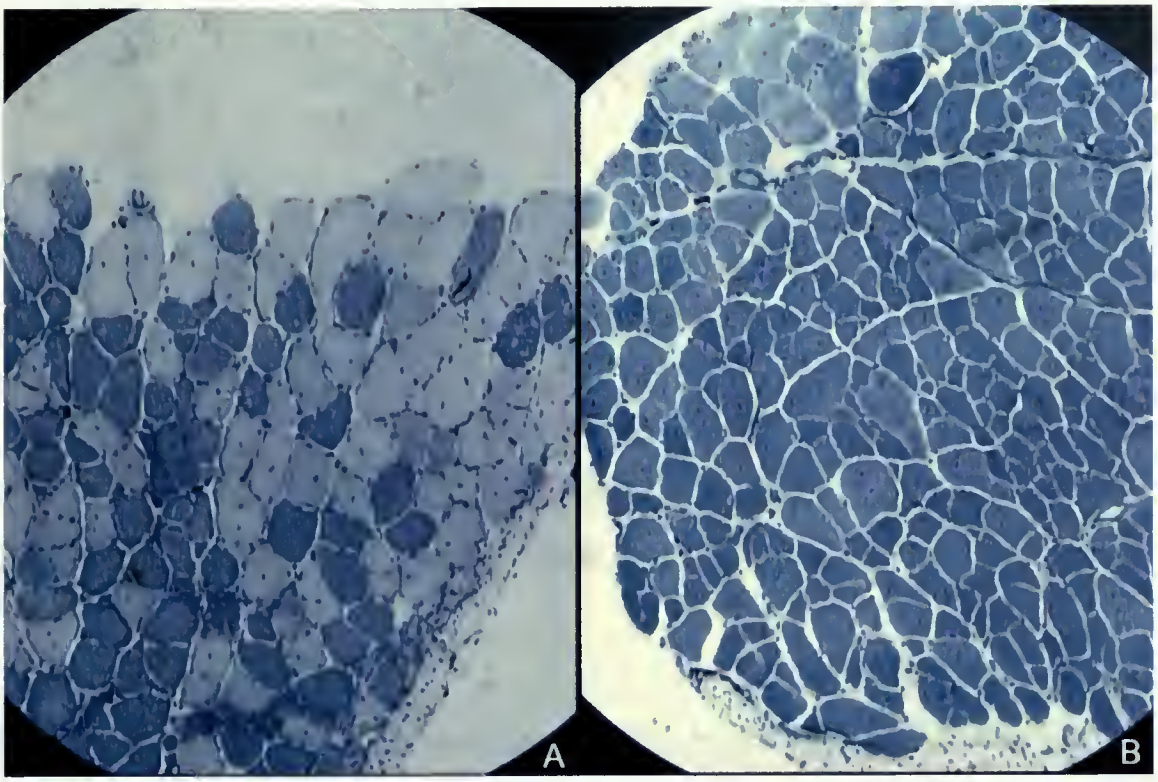

Figure 6.1: Cross sections of 10 month old *mdx* mouse soleus (panel A) and EDL (panel B) showing ATPase activity following pre-incubation at pH 4.55, incubation at pH 9.4 with ATP and staining with Azure A. The lightly coloured cells in panel A indicate the presence of type IIA fibers. These cells are not present in panel B suggesting that there are no IIA fibers in the EDL muscle.

Potentiation is graded to myosin light chain phosphorylation levels (110). An increase in potentiation could be due to greater RLC phosphorylation or increased Ca^{2+} influx into the cytosol. In resting skeletal muscle, baseline levels of phosphorylated RLC are at very low levels (109). It does not seem likely that there are differences in baseline phosphorylation in this experiment, as the twitch to tetanus ratios are equal in all conditions (figure 6.2). Higher values in a condition could have indicated that there was a certain amount of baseline phosphorylation and potentiation.

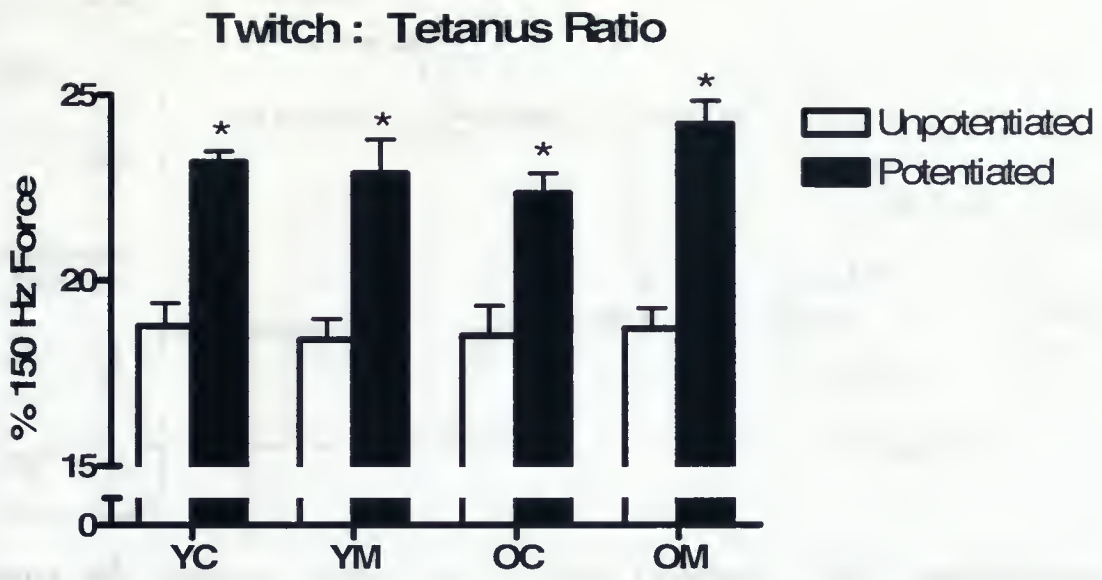

Figure 6.2: Ratio of maximum force during unpotentiated and potentiated twitches to maximum force at 150 Hz.

* Significantly higher than unpotentiated twitch: tetanus ratio ($p<0.001$)

Following an excitatatory stimulation, Ca^{2+} is released into the cytosol. This Ca^{2+} binds to CaM which goes on to activate skMLCK. Myosin RLC is phosphorylated by activated skMLCK, leading to myosin heads exhibiting faster transitions from the non-force producing state to the force producing state, ultimately increasing the number of cross-bridges in the force producing state at any given submaximal Ca^{2+} concentration. $PP1_M$ is constantly opposing skMLCK by dephosphorylating the RLC. This relationship is described in figure 6.3. Factors that can affect the proportion of RLC in the phosphorylated state include: intracellular Ca^{2+}, concentrations of CaM in the activated state and concentrations and activity of skMLCK and $PP1_M$.

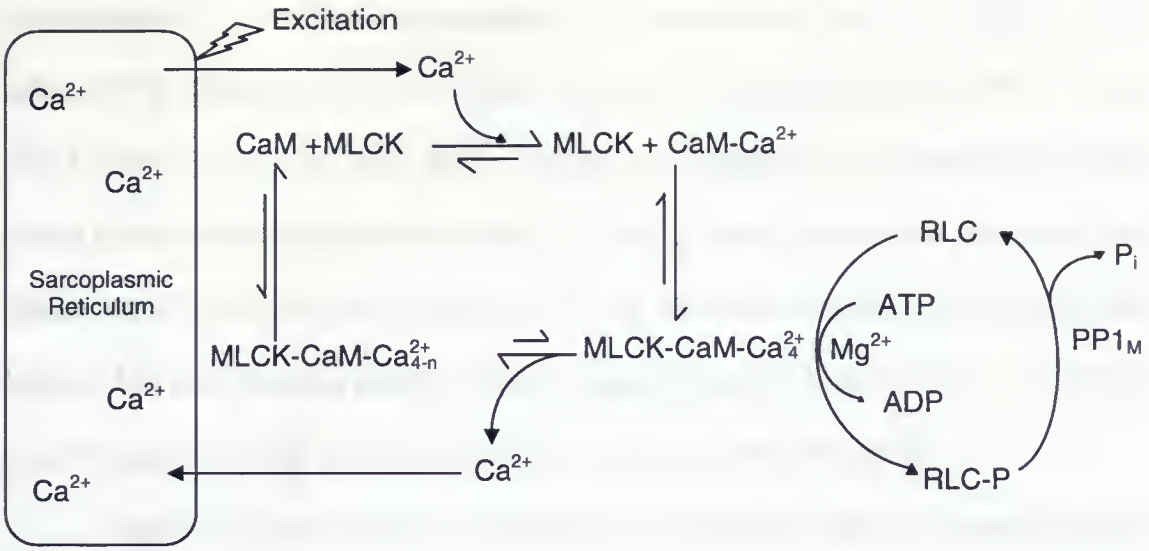

Figure 6.3: Based on Sweeney *et al.* (101). Flowchart of RLC phosphorylation regulation. Following excitation either by surface stimulation or action potential, Ca^{2+} binds to CaM after being released from the SR. This Ca^{2+}-CaM complex binds to and activates MLCK. Activated MLCK phosphorylates the myosin RLC using a molecule of ATP in the process. When $[Ca^{2+}]_c$ drops, Ca^{2+} dissociates from CaM over the course of a few seconds, causing CaM to dissociate from MLCK, preventing further RLC phosphorylation. Throughout this process, $PP1_M$ dephosphorylates phosphorylated RLC, albeit at a much lower rate than that of RLC phosphorylation by activated MLCK.

Elevated potentiation in *mdx* mice cannot be explained by skMLCK expression levels in whole muscle, as there were no significant differences due to age or the *mdx* condition. Determination of fiber type dependent expression of skMLCK using immunohistochemical techniques is not possible using antibodies currently on the market due to the presence of non-specific binding which may be fiber type dependent. Efforts were made to determine $PP1_M$ expression; however this was confounded by a

combination of factors. $PP1_M$ is composed of a regulatory unit and the 37 kDa catalytic subunit $PP1_\beta$. The combined mass of these subunits has been reported as 60 kDa, but may also be between 100-150 kDa due to suspected proteolysis of the regulatory subunit during trypsin digestion used in the study (27). There was no band visible on the Western blots at 60 kDa, nor was there a band at 37 kDa, and there were several bands between 100 and 150 kDa (data not shown). Further compounding the difficulties, $PP1_\beta$ is also the catalytic subunit seen in the glycogen-associated protein phosphatase (8).

Older mice were heavier in both *mdx* and control mice. This is an expected result since younger mice do not reach full mass until 6 months of age (60). Contrary to published findings (60), no differences in whole body mass were seen at 10 months of age. Beyond 6 months of age, *mdx* mice are generally lighter than age matched controls (60). The discrepancies in this study may be attributed to the small sample size used or the housing of the mice, as OM were housed individually and OC were housed in groups of 4. In accordance with published literature, *mdx* mice were heavier than controls at 50 days (116). This increased mass can be identified as pseudohypertrophy reported in young dystrophic muscle in previous studies due to large necrotic regions and accumulation of connective tissue and fat (60; 61; 97; 100).

Individual muscle masses and lengths were not recorded; as such normalization to CSA is not possible. The effect of age on force production can be explained by muscle size and the assumption that a heavier mouse can be expected to have larger muscles than a lighter mouse. Previous studies have found that *mdx* muscle is larger than control muscle (60; 89), and that absolute forces are comparable to control muscle (5; 77; 79; 89). In the present study, forces generated by *mdx* EDL were found to be lower than

control EDL at all stimulation frequencies. This can be explained by a study that found that free access to a running wheel has been shown to reduce strength and increase damage in EDL muscles of old *mdx* mice with no effect on young mice (16). This damage can manifest as pseudohypertrophy of *mdx* muscle, where a significant portion of the CSA consists of regions of reduced or no force production including: mononuclear cells, degenerating or branched cells, connective tissue, fat (5; 6; 60; 61; 97). Each of these factors could also explain why YM exhibited lower forces than YC. Additionally, since these mice are in a period of fiber regeneration, the presence of relatively weak embryonic or neonatal myosin isoforms may contribute to the lower absolute force (21; 79).

Although measures of cell damage or viability were not made, regions consisting of mononuclear cells, connective tissue and degenerated cells can be seen in cross sectional images of *mdx* fibers (panels C and D, figure 5.12). Branching of fibers is suggested by regions containing very small cells in panel D. Force normalized to CSA is lower in *mdx* mice (5; 29; 79; 89; 97; 98). Each of these factors can reduce the force to CSA ratio leading to the lower forces seen in *mdx* EDL in this study.

The potentiated state of skeletal muscle myosin may be the more physiologically important state during physical activity as survival can often depend on the first 30 seconds of activity whether as predator or prey. As such, it would be advantageous for a muscle in the natural environment to maintain performance rather than minimizing damage, even in a diseased state.

OM did not show greater fatigue resistance than OC as previously reported (29; 79; 83; 89) as would be expected from having a slower fiber type profile associated with greater fatigue resistance, though YM did have improved fatigue resistance but did not exhibit different fiber type profiles than age matched controls. This appears to be caused by a right shift in the force frequency curve in YM muscle. Using only trials that permitted 150 Hz contraction, the ratio of 40 Hz to 150 Hz for YM is 0.51 ± .03, while for YC, OC and OM this ratio is 0.66 ± 0.026, 0.68 ± 0.034 and 0.63 ± 0.030 (figure 6.5). This right shift in the force frequency curve is perfectly consistent with the findings of Sacco *et al.* (89) who reported that 40 Hz stimulation corresponds to 70% and 55% of 100 Hz force in C57 mice and *mdx* mice respectively.

By shifting the force frequency curve to the right, the YM EDL is performing less relative work and is therefore able to exhibit less fatigue at the same contraction frequency. In a study by Petrof *et al.* (79) showed that when compared to controls, the force frequency curve of 24 month old *mdx* diaphragm is left shifted in response to a shift to slower myosin isoforms. The study by Sacco *et al.* did not examine mice older than 5 months of age, so it is possible that these mice would also have exhibited a left shift in the force frequency curve had they looked at older mice.

The fiber type changes are not as severe in limb muscle as in diaphragm, nor did the current study examine mice as old as 24 months. It seems likely that over the lifespan of an *mdx* mouse there is a progressive shift to the left in the force frequency relationship in response to a gradual shift in fiber type. Sacco *et al.* reported lower TPT in twitches of *mdx* mice (89) as a cause of the right shift in the force-frequency curve of *mdx* muscle. A reduction in TPT was also seen in YM during unpotentiated twitches and in both young

and old *mdx* mice during tetanic contractions. Lower TPT seen in YM in this study does not appear to be due to be a function of force in unpotentiated twitches as all other groups exhibited similar values for TPT regardless of the force produced.

One hypothesis for faster TPT in *mdx* muscle is that dystrophin may play a role in force development by acting as a dampener. Some of the initial energy produced by muscle may be expended by deformation and stretching of dystrophin and its anchored structures, which are radial to the direction of pull (78). In the absence of dystrophin, the energy may be passed along the series elastic component faster, leading to faster TPT. Figure 6.4 supports this idea as the $+df/dt$ controlled for force is greater in *mdx* mice than in age matched controls, suggesting that force is more efficiently distributed longitudinally in *mdx* muscle. In dystrophic muscle, the contractile elements of muscle may essentially abandon the sarcolemma and basal lamina in the initial stages of contraction, leaving other structures such as myofilaments to maintain proper orientation of the basal lamina and sarcolemma with respect to the contractile elements. This could partially explain the fiber type specific damage seen in muscular dystrophy, as a faster, more powerful contraction could surpass the ability of the sarcolemma to absorb the force applied through the myofilaments, creating a wound. This would be especially true during eccentric contractions when compression of the myofilament lattice is greatest and radial forces are highest (17; 78). This seems to be further supported by the absence of utrophin in fast fibers, which has been shown to stabilize the dystrophin complex when present, providing an additional path through which the force can be distributed (18; 19).

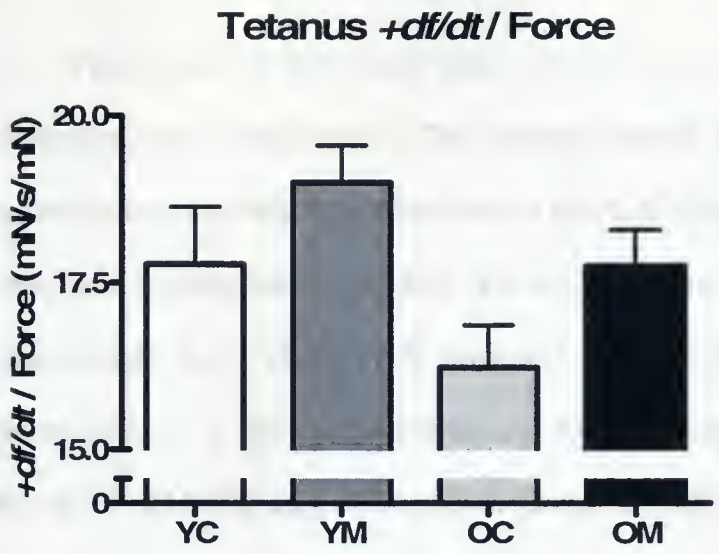

Figure 6.4: Rate of force production normalized to force in tetanic stimuli.

Main effect of age was significant (Young > old, $p<0.05$)

Main effect of condition was significant (*mdx* > control, $p<0.05$)

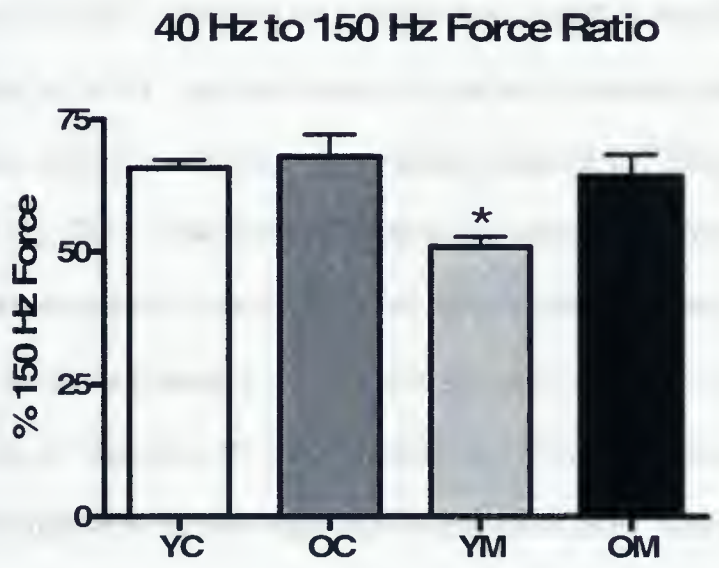

Figure 6.5: Ratio of maximum force at 40 Hz to maximum force at 150 Hz. YC: n=7; OC: n=4; YM: n=6; OM: n=6.

* Significantly lower than OM ($p<0.05$) and YC ($p<0.01$)

The results of this study can not explain the mechanism behind elevated potentiation seen in *mdx* muscle. This warrants further investigation. Other avenues to explore include the phosphorylation level of the RLC. This would identify if potentiation is due to RLC phosphorylation alone or if there are other contributing factors. Although whole muscle levels of skMLCK were not significantly different between *mdx* and control mice, it is possible that there are fiber type specific changes in expression. Activity of skMLCK may be increased in *mdx* muscle, providing an explanation for elevated potentiation without requiring elevated skMLCK expression. It is unlikely that $PP1_M$ plays a large role in defining the maximum level of potentiation as the relative drop in potentiated force was faster in the most highly potentiated muscles (figure 5.5), which may be due to enzyme kinetics and not a change in protein expression or maximal activity. Ca^{2+} transients may be the most important aspect to explore. It has been found that while Ca^{2+} release induced by surface stimulation does not differ between control and *mdx* EDL muscle, action potential induced Ca^{2+} release is impaired in *mdx* muscle (117). This impairment is marked by reduced amplitude of Ca^{2+} transients and by increased duration of the decay of these transients. When also considering the right shift in the force frequency curve seen in young *mdx* muscle and that physiological stimulation rate is less than 50 Hz (reviewed in (52)), *mdx* muscle would appear to be quite insensitive to its own signaling. Therefore in order to reach functionally adequate force levels, the *mdx* mouse has two options: increase muscle mass or increase sensitivity to action potentials. Increasing muscle would have a significant metabolic cost both to build and maintain and would hardly be practical due to the high degree of muscle regeneration

required due to the disease condition. Increasing sensitivity to action potentials can be done by phosphorylation of the myosin RLC, which has the effect of increasing Ca^{2+} sensitivity. The extra metabolic load of phosphorylated myosin is minimal compared to muscle hypertrophy, since phosphorylation dissipates after 10-20 minutes of inactivity. Therefore force potentiation may be vital for reaching physiological force levels in the *mdx* mouse.

A second option for increasing sensitivity to action potentials is to increase the Ca^{2+} signal released following an action potential. Ca^{2+} transients may play an important role in potentiation as Decostre *et al.* (25) have found that the peak $[Ca^{2+}]_c$ concentration is higher following a conditioning stimulus in isolated mouse EDL. EDL of skMLCK knockout mice subjected to repetitive stimulation at 10 Hz, show a progressive increase in twitch force while these same mice do not exhibit post-tetanic potentiation (118). This suggests that there is a skMLCK independent mechanism that can cause force potentiation. It has been suggested that CaM may have an excitatory effect on ryanodine and dihydropyridine receptors that cause increased amounts of Ca^{2+} to be released per stimulus, making more Ca^{2+} available to activate contractile proteins. There may also be an increase in resting Ca^{2+} levels after a conditioning stimulus that could contribute to force potentiation (25).

It has been shown that skMLCK activity is the limiting factor in frequency dependent phosphorylation of the RLC in wild type mice and that CaM supplies are only limiting in transgenic mice expressing 22 fold greater concentrations of skMLCK (88). Since *mdx* mice do not exhibit greater whole muscle expression of skMLCK than controls and CaM does not limit RLC phosphorylation (88), there must be differences in

Ca^{2+} transients that affect CaM-skMLCK interactions. The CaM-Ca^{2+}-skMLCK complex both forms and dissociates more slowly than the Ca^{2+}-troponin complex (reviewed in (33)). Previous studies have shown that amplitudes of Ca^{2+} transients in *mdx* mice using surface stimulation are either identical to (43; 107; 117) or larger than (104; 106) those of control mice. Ca^{2+} transients have also been reported to have a longer decay phase in *mdx* than control mice (104; 107) in response to higher resting $[Ca^{2+}]_c$ (104) which is commonly seen in dystrophic muscle (48; 63; 106). A larger or slower Ca^{2+} transient would provide greater opportunity for the CaM-Ca^{2+}-skMLCK complex to form, potentially increasing the amount of activated skMLCK available to phosphorylate the RLC leading to greater force potentiation in the *mdx* mouse.

It is unlikely that parvalbumin play a role in PTP. This cytosolic protein acts as a temporary Ca^{2+} buffer during contraction, facilitating relaxation. In parvalbumin +/- and -/- mice, twitch force, TPT and 1/2RT are all increased (93). These changes would not be altered by the contractile measurements in this study as $[Ca^{2+}]_c$ returned to baseline within 0.25 s following a 50 ms stimulation (93), though it may play a larger role in staircase potentiation due to the rapid succession of twitches. Anderson *et al.* have reported that there are no changes in parvalbumin content between 4 and 32 week old control and *mdx* mice (5).

Since myosin phosphorylation acts through an increase in *+df/dt*, it is noteworthy that increases in *+df/dt* did not increase proportionally to the amount of potentiation seen in this study, Average baseline-normalized increases in *+df/dt* during potentiated twitches for every group were 23-24 ± 1.0-1.5%. It is noteworthy that normally *+df/dt* increases to a greater extent than force following a conditioning stimulus (108), however in OM force

potentiated more than *+df/dt*. Additionally, the baseline-normalized changes in maximum rates of relaxation were markedly different between *mdx* and control conditions with the magnitude of *-df/dt* increasing by 48 ± 9% in YM, 40 ± 7% in OM, 31 ± 6% in YC and 30 ± 5% in OC. This suggests that there are differences in Ca^{2+} handling between *mdx* and control mice during potentiated twitches. These changes are most likely to be mediated by CaM acting on the release channel.

In accordance with previous literature (5), the older mice had faster 1/2RT, fewer slow twitch fibers and increased force potentiation compared to young mice. Contrary to literature (5), TPT was not slowed with age in control mice.

Chapter 7

I. Limitations:

This study only examines functional aspects of potentiation in *mdx* EDL. Mechanisms behind elevated potentiation in *mdx* muscle are better examined using measurements of Ca^{2+} transients and phosphorylation of the myosin RLC in addition to force measurements. Muscle from this study has been fast frozen for RLC analysis at a future date. This data may shed some light on mechanisms behind increased potentiation seen in *mdx* mice.

Activity of skMLCK and $PP1_M$ were not measured. There may be differences in the degrees of activation of these proteins.

Fiber type specific changes in skMLCK or $PP1_M$ content were not possible to measure. There may be fiber type specific changes in the expression of these proteins that are not discernable from whole muscle homogenate.

Potentiation exists concurrently with fatigue. No measurements were taken to determine how fatiguing the conditioning stimulus was for each condition. This could have been done by performing a tetanic stimulation following the end of the conditioning stimulus. Vandenboom *et al.* (110) have shown that this CS results in ~22% depression in P_o. It is possible that the differences in potentiation seen in this experiment are actually a less fatiguing conditioning stimulus in the *mdx* conditions. This does not seem likely as the time to 50% force during constant 40 Hz stimulation was longer in only the young *mdx* condition. Therefore a more plausible scenario would involve the CS being less fatiguing for the 50 day old *mdx* muscles compared to the other groups and perhaps a greater degree of phosphorylation in the 10 month old *mdx* group. Measurement of muscle metabolites could also have given insights in to the fatigability of the muscles, however due to the small size of the mouse EDL and the desire to use some muscle to determine RLC phosphorylation in the future, this was not possible.

II. Summary:

The EDL of the *mdx* mouse potentiates more than that of the control mouse at ages 50 days and 10 months. This may be compensatory for the reduced forces seen in *mdx* mice at every contraction frequency examined.

Old *mdx* EDL has a lower proportion of IIB fibers than control EDL or young *mdx* EDL.

No changes were seen in expression of skMLCK at the whole muscle level.

Young *mdx* muscle fatigued more slowly than old *mdx* and control mice. This corresponded to a reduction in time to peak tension and reduced ratio of force at 40Hz to force at 150Hz in the young *mdx* group.

III. Conclusions:

Old *mdx* mice exhibit greater force potentiation than either old control mice or young *mdx* mice in response to a conditioning stimulus. This occurs in spite of fiber type shifts toward slower fiber types. The increased potentiation is not due to changes in skMLCK expression as there were no differences seen between groups. It is uncertain at this time whether increased potentiation in *mdx* mice is due solely to greater phosphorylation of the myosin regulatory light chain or if there are differences in Ca^{2+} transients following a conditioning stimulus that also lead to increased forces. Since potentiation is elevated in old mdx mouse muscle, further study is necessary to determine its functional purpose before either using or avoiding it in exercise prescriptions as treatment for those with DMD. Another interesting finding is that the 40 Hz to 150 Hz force ratio is reduced in young *mdx* mice but not old *mdx* mice. This is supported by increased time to fatigue at 40 Hz and reduced TPT in twitches in young *mdx* mice.

Appendix 1

Western Blotting Buffers

4X Running Gel Buffer Stock: 1.5 M Tris-HCl, pH 8.8 (100 mL)

18.16 g Tris base (1.5 M)

0.40 g SDS (0.4%)

Add ~48 mL of 1M HCl and mix

Bring to 100 mL final volume with distilled water

Titrate the solution to pH 8.8

Filter the solution through a Whatman No. 1 filter paper

Store at 4°C for up to 1 month

4X Stacking Gel Buffer Stock: 0.5 M Tris-HCl, pH 6.8 (100 mL)

6.06 g Tris base (0.5 M)

0.40 g SDS (0.4%)

Add 40 mL of distilled H_2O

Titrate to pH 6.8 with 1 M HCl (~48 mL)

Bring to 100 mL final volume with distilled water

Filter the solution through a Whatman No. 1 filter paper

Store at 4°C for up to 1 month

10% Ammonium Persulfate Solution (APS)

0.05 g Ammonium persulfate

Dissolve in 400 µL distilled water

Dilute to 500 µL with distilled water

Store at 4°C up to 1 week

2X Sample Buffer

5.0 mL 1.25 M Tris-HCL Buffer, pH 6.8

2.0 g SDS

5.0 mL 2-Mercaptoethanol

11.6 mL Glycerol (87%)

10 mg Bromophenol Blue

Make up to 50 mL with distilled H_2O

Stir until all SDS and Bromophenol blue has dissolved

Store at room temperature for 4 weeks or at -20°C in 1-5 mL aliquots for 4-6 months

10X Electrode Buffer, Tris/Glycine

144.2 g Glycine

30.3 g Tris base

10.0 g SDS

Dissolve in 800 mL distilled water

Make up to 1 L with distilled water

Store at room temperature for up to 2 months

pH should be ~8.3 without adjustment

Each day dilute 100 mL of 10X electrode buffer to 1000 mL with distilled water to get 1X electrode buffer

Transfer Buffer

6.055 g 25 mM Tris base

28.53 g 192 mM Glycine

400 mL 10% v/v Methanol

Dilute to 2 L

Do not adjust pH

10X Tris-Buffered Saline (TBS), pH 7.5

48.44 g 200 mM Tris base

160.3 g 1.37 M NaCl

76.0 mL HCl

Dilute to 2 L with distilled water

Adjust pH to 7.5

Store at 4°C up to 1 month

Each day take 100 mL of 10X TBS and dilute to 1 L with distilled water to make 1X TBS pH 7.5

0.1% TBS-T (Washing Buffer)

1 mL Tween-20

Add to 1 L 1X TBS and mix well

Keep at 4°C when not in use

7.5 % Running Gel - 1 Set

H_2O 7.5 mL

30% Acrylamide 3.75 mL

4X Running Gel 3.75 mL

10% APS 75 µL

TEMED 7.5 µL

Stacking Gel - 1 Set

H_2O 4.6 mL

30% Acrylamide 1.0 mL

4X Stacking Gel 1.9 mL

10% APS 38 µL

TEMED 7.5 µL

Appendix 2

Western Blotting Procedure

Setting up the Apparatus

1. Clean the glass plates with distilled water. Make sure they are clean and dry before proceeding.
2. Place glass plates in the gel-forming apparatus with the thick plate towards the back. Work on a level surface.

Running Gel

1. Add distilled water, 30% acrylamide and 4X running buffer according to instructions in Appendix 1 in a small Erlenmeyer flask and mix together by gentle swirling.
2. Add 10% APS and TEMED according to instructions in Appendix 1 into Erlenmeyer flask and mix by gentle swirling.
3. Mix everything using a syringe.
4. Inject the gel into plates with a soft syringe tip until the gel reaches ~2 cm below the top of the glass, touching the tip of the syringe to the glass.
5. Wash syringe with distilled water.
6. With small syringe inject a layer of distilled water on top of the gel. This prevents air from contacting the gel, allowing polymerization to take place.
7. Wait 40 minutes for gel to polymerize.

Stacking Gel

1. Once the gel has polymerized, use filter paper to soak up the water.
2. Add distilled water, 30% acrylamide and 4X stacking buffer according to instructions in Appendix 1 in a small Erlenmeyer flask and mix together by gentle swirling.
2. Add 10% APS and TEMED according to instructions in Appendix 1 into Erlenmeyer flask and mix by gentle swirling.
3. Mix everything using a syringe.
4. Inject the gel into plates with a soft syringe tip up to the top of the glass. Use a kimwipe at the bottom of the plates to catch any excess gel.
5. Wash syringe with distilled water.
6. Insert comb between plates such that the notch goes over the thin plate.
7. Wait 40 minutes for gel to polymerize.

Sample Loading

1. Remove combs to reveal indents in the gel.
2. Insert plates into electrode apparatus such that the thin plates face the center of the apparatus. Be sure plates are labeled.
3. Fill wells with 1X electrode buffer to the top of the plates.
4. First and last wells are filled with 2X sample buffer (~10 µL)
5. 3.5 µL of protein marker goes in 2nd well.
6. Use drawn out Eppendorf pipette tips to insert samples in wells.

Don't overload the wells or the bands will be distorted.

Don't underload the wells or the bands will be too faint.

Be sure the tip of the pipette is 1-2 mm above the gel surface to minimize sample mixing with the reservoir buffer during loading.

Empty wells are filled with 2X sample buffer.

7. Put electrode apparatus into electrophoresis tank ½ full of 1X electrode buffer.

   Fill between plates with to the top of the plates.

   Fill outside the electrode above the base of the plates.

8. Use bent syringe to remove any air bubbles at the base of the plates.
9. Place lid on the electrophoresis tank matching red to red and black to black, ensuring proper electrical flow.
10. Set voltage to 110 V and wait ~1 hour until the blue dye reaches the bottom edge of the plate.

Preparing the Membrane and Filter Paper

1. Cut two pieces of polyvinylidene difluoride membrane to the size of the gel and notch the corners to identify gels. Do not touch the membrane with hands.
2. Activate the membranes by immersing them in 100% methanol for a few seconds, rinse well with distilled water, then equilibrate with transfer buffer for a few minutes.
3. Completely saturate pre-cut pieces of Whatman filter paper and fiber pads by soaking them in cold transfer buffer. Avoid trapping air bubbles in the pads or paper during the wetting process.

Trans Blot Semi-Dry Apparatus

1. Unplug and turn off apparatus.
2. Pour buffer that was between plates out as waste. Buffer on the outside of the plates can be reused.
4. Remove the plates from the electrodes.
5. Cut off excess gel using a plastic edge.
6. Notch the gel for identification purposes.
7. Put the gel into a dish with transfer buffer and equilibrate 15 minutes. This facilitates removal of electrophoresis buffer salts and detergents and allows the gel to adjust to its final size prior to transfer.
8. Place thick blot pad on the center of the anode plate and roll out excess fluid and trapped air with a test tube.
9. Place thin blot paper on top of thick blot pad. Roll out air and excess fluid with a test tube.
10. Place membrane on thin blot paper. Roll out air and excess fluid with a test tube.
11. Place gel on membrane. Roll out air and excess fluid with a test tube.
12. Place thin blot paper on membrane. Roll out air and excess fluid with a test tube.
13. Place thick blot pad on thin blot paper. Roll out air and excess fluid with a test tube.
14. Place cathode on top, ensuring the white latches are in place.
15. Plug in apparatus matching red to red and black to black.
16. Set voltage to 23 V.
17. Set time to 40 minutes (2 gels).

Antibodies

1. Unplug and turn off apparatus.
2. Return blotting papers to buffer.
3. Gels go in waste bucket.
4. Allow membrane to dry 5-10 minutes - can be kept up to 1 month if it is kept clean.
5. Block non-specific binding sites with 5% bovine serum albumin in TBS-T, shaking gently for 1 hour.
6. Pour off blocking solution and add first antibody solution (8 mL/membrane). This is a dilution of the blocking solution.
7. Incubate for 1 hour with gentle shaking at room temperature.
8. Decant the primary antibody solution. This can be reused several times.
9. Wash for 30 minutes with fresh changes of washing buffer every 5 minutes using gentle shaking.
10. Dilute secondary antibody in TBS-T (1:7500)
11. Incubate the membrane in diluted secondary antibody for 1 hour with gentle shaking at room temperature.
12. Decant the secondary antibody solution. Do not reuse.
13. Wash for 30 minutes with fresh changes of washing buffer every 5 minutes using gentle shaking at room temperature.

Enhanced Chemiluminescence (ECL) Immunodectection Procedure

1. Take the ECL detection reagents and mix 0.75 mL of reagent 1 and 0.75 mL reagent 2 in a test tube.

2. Drain excess TBS-T from the membrane.
3. Pour detection mixture directly on the membrane surface with the protein. Do not let the blot dry.
4. Incubate for 1 minute precisely at room temperature while shaking gently.
5. Drain off excess detection reagent mixture using a kimwipe.
6. Gently place the blot protein side down on a sheet of plastic wrap. Gently smooth out any air pockets.

Syngene Machine

1. Click on GeneSnap on the desktop.
2. Click the green button.
3. Select "upper white" to see the blot.
4. Place the blot protein side up in the machine using the screen to guide the placement.
5. Select "no light" and series capture to 5.
6. Set the exposure times to vary between 30 s and 2 minutes.
7. Once the pictures appear, adjust the contrast to get a clear image.

Wash all equipment thoroughly with water and a scrub brush.

Appendix 3

Myosin ATPase Azure A Protocol

Reagents

1. Basic Medium	53 mM Glycine	FW 75.1	3.96 g
	38 mM Calcium Chloride	FW 111.0	4.20 g
	65 mM Sodium Chloride	FW 58.44	3.80 g
	25 mM Sodium Hydroxide	FW 40.0	1.90 g
	Distilled H_2O		1.0 L

Add all reagents except calcium chloride and dissolve, then add calcium chloride. Store at room temperature for 30 days or until cloudy.

2. Acid Medium	100 mM Sodium Acetate	FW 136.08	6.47 g
	100 mM Potassium Chloride	FW 74.56	3.70 g
	Distilled H_2O		500 mL

Store at room temperature for up to 30 days.

3. Azure A	1% Azure A (C.I. 52005)	200 mg
	Distilled H_2O	20 mL

Reuse four or five times

Working Reagents

1. pH 4.55 Pre-incubation Medium		Acid Medium	30 mL

Bring to pH 4.55 with Acetic Acid

2. pH 10.3 Pre-incubation Medium		Basic Medium	30 mL

Bring to pH 10.3 with 1.0 M HCl *** Do not go below pH 10.3

3. Pre-incubation Wash		Basic Medium	100 mL

Bring to pH 9.4 with 1.0 M HCl *** Do not go below pH 9.4

4. Incubation Medium	30 mM ATP	FW 605.2	51 mg
		Basic Medium	30 mL

Stir for 2 minutes, then bring to pH 9.4 with 1.0 M HCl *** Do not go below pH 9.4

* pH this reagent last as it clogs the pH electrode. Soak pH electrode in 0.1 M HCl following this final pH

Procedure

1. Remove sections from freezer and bring to room temperature.
2. All steps are done on a shaker. Place slides in a columbia jar.

3a) Add 4.55 Pre-incubation Medium for 150 seconds (25°C)

b) Add 10.3 Pre-incubation Medium for 45 seconds (37°C)

4. Rinse 2 times for 30 seconds with Pre-incubation Wash (25°C)
5. Incubate for 20 minutes in Incubation Medium (37°C)

6. Rinse in 1% Azure A for 20 seconds (25°C)

7. Wash well with deionized water.

8. Rinse in 80% Ethanol for 2 minutes.

9. Rinse in 90% Ethanol for 2 minutes.

10. Rinse in 100% Ethanol for 2 minutes.

11. Rinse twice in Xylene for 2 minutes.

12. Mount in Permount.

Stain	I	IIA	IIX/D	IIB
10.3	Light	Dark	Dark	Dark
4.55	Dark	Light	Medium	Dark

1. **Abbate F, Sargeant AJ, Verdijk PWL and de Haan A**. Effects of high-frequency initial pulses and posttetanic potentiation on power output of skeletal muscle. *J Appl Physiol* 88: 35-40, 2000.

2. **Agbulut O, Noirez P, Beaumont F and Butler-Browne GS**. Myosin heavy chain isoforms in postnatal muscle development of mice. *Biology of the Cell* 95: 399-406, 2003.

3. **Albrecht DE and Froehner SC**. Syntrophins and dystrobrevins: defining the dystrophin scaffold at synapses. *Neurosignals* 11: 123-129, 2002.

4. **Allen DG, Lännergren J and Westerblad H**. Muscle cell function during prolonged activity: cellular mechanisms of fatigue. *Exp Physiol* 80: 527, 1995.

5. **Anderson JE, Bressler BH and Ovalle WK**. Functional regeneration in the hind limb skeletal muscle of the *mdx* mouse. *J Muscle Res Cell Motil* 9: 499-515, 1988.

6. **Anderson JE, McIntosh LM, Moor AN and Yablonka-Reuveni Z**. Levels of MyoD protein expression following injury of *mdx* and normal limb muscle are modified by thyroid hormone. *J Histochem Cytochem* 46: 59-67, 1998.

7. **Armstrong RB and Phelps RO**. Muscle fiber type composition of the rat hind limb. *Am J Anat* 171: 259-272, 1984.

8. **Berndt N, Campbell DG, Cauldwell FB, Cohen P, da Cruz e Silva EF, da Cruz e Silva OB and Cohen PT**. Isolation and sequence analysis of a cDNA clone encoding a type-1 protein phosphatase catalytic subunit: homology with protein phosphatase 2A. *FEBS Lett* 223: 340-346, 1987.

9. **Bourke DL and Ontell M**. Branched myofibers in long-term whole muscle transplants: a quantitative study. *Anat Rec* 209: 281-288, 1984.

10. **Bozzo C, Spolaore B, Toniolo L, Stevens L, Bastide B, Cieniewski-Bernard C, Fontana A, Mounier Y and Reggiani C**. Nerve influence on myosin light chain phosphorylation in slow and fast skeletal muscles. *FEBS J* 272: 5771-5785, 2005.

11. **Brenner B**. Effect of Ca^{2+} on cross-bridge turnover kinetics in skinned single rabbit psoas fibers: implications for regulation of muscle contraction. *Proc Natl Acad Sci U S A* 85: 3265-3269, 1988.

12. **Brooks SV and Faulkner JA**. Contractile properties of skeletal muscles from young, adult and aged mice. *J Physiol* 404: 71-82, 1987.

13. **Brown IE and Loeb GE**. Measured and modeled properties of mammalian skeletal muscle. I. The effects of post-activation potentiation on the time course and velocity dependencies of force production. *J Muscle Res Cell Motil* 20: 443-456, 1999.

14. **Bulfield G, Siller WG, Wight PAL and Moore KJ**. X chromosome-linked muscular dystrophy (*mdx*) in the mouse. *Proc Natl Acad Sci USA* 81: 1192, 1984.

15. **Carnwath JW and Shotton DM**. Muscular dystrophy in the *mdx* mouse: histopathology of the soleus and extensor digitorum longus muscles. *J Neuro Sci* 80: 39-54, 1987.

16. **Carter GT, Wineinger MA, Walsh SA, Horasek SJ, Abresch RT and Fowler WM**. Effect of voluntary wheel-running exercise on muscles of the *mdx* mouse. *Neuromuscular Disorders* 5: 323-332, 1995.

17. **Cecchi G, Bagni MA, Griffiths PJ, Ashley CC and Maeda Y**. Detection of radial crossbridge force by lattice spacing changes in intact single muscle fibers. *Science* 250: 1409-1411, 1990.

18. **Chakkalakal JV, Michel SA, Chin ER, Michel RN and Jasmin BJ**. Targeted inhibition of Ca^{2+}/calmodulin signaling exacerbates the dystrophic phenotype in *mdx* mouse muscle. *Human Molecular Genetics* 15: 1423-1435, 2006.

19. **Chakkalakal JV, Stocksley MA, Harrison MA, Angus LM, Deschenes-Furry J, St Pierre S, Megeney LA, Chin ER, Michel RN and Jasmin BJ**. Expression of utrophin A mRNA correlates with the oxidative capacity of skeletal muscle fiber types and is regulated by calcineurin/NFAT signaling. *Proc Natl Acad Sci U S A* 100: 7791-7796, 2003.

20. **Clarke MS, Khakee R and McNeil PL**. Loss of cytoplasmic basic fibroblast growth factor from physiologically wounded myofibers of normal and dystrophic muscle. *J Cell Sci* 106: 121-133, 1993.

21. **Coirault C, Lambert F, Marchand-Adam S, Attal P, Chemla D and Lecarpentier Y.** Myosin molecular motor dysfunction in dystrophic mouse diaphragm. *Am J Physiol Cell Physiol* 277: C1170-C1176, 1999.

22. **Coirault C, Samuel JL, Chemla D, Pourny JC, Lambert F, Marotte F and Lecarpentier Y.** Increased compliance in diaphragm muscle of the cardiomyopathic Syrian hamster. *J Appl Physiol* 85: 1762-1769, 1998.

23. **Corrado K, Rafael JA, Mills PL, Cole NM, Faulkner JA, Wang K and Chamberlain JA.** Transgenic *mdx* mice expressing dystrophin with a deletion in the actin-binding domain display a "mild Becker" phenotype. *J Cell Biol* 134: 873-884, 1996.

24. **Deconinck N, Tinsley J, de Backer F, Fisher R, Kahn D, Phelps S, Davies K and Gillis JM.** Expression of truncated utrophin leads to major functional improvements in dystrophin-deficient muscles of mice. *Nat Med* 3: 1216-1221, 1997.

25. **Decostre V, Gillis JM and Gailly P.** Effect of adrenaline on the post-tetanic potentiation in mouse skeletal muscle. *J Muscle Res Cell Motil* 21: 254, 2000.

26. **Delbono O, O'Rourke KS and Ettinger WH.** Excitation-calcium release uncoupling in aged single human skeletal muscle fibers. *J Membr Biol* 148: 211-222, 1995.

27. **Dent P, MacDougall LK, Mackintosh C, Campbell DG and Cohen P.** A myofibrillar protein phosphatase from rabbit skeletal muscle contains the β isoform of protein phosphatase-1 complexed to a regulatory subunit which greatly enhances the dephosphorylation of myosin. *Eur J Biochem* 210: 1037-1044, 1992.

28. **DiMario JX, Uzman A and Strohman RC.** Fiber regeneration is not persistent in dystrophic (*mdx*) mouse skeletal muscle. *Dev Biol* 148: 314-321, 1991.

29. **Dupont-Versteegden EE and McCarter RJ.** Differential expression of muscular dystrophy in diaphragm versus hind limb muscles of *mdx* mice. *Muscle Nerve* 15: 1105-1110, 1992.

30. **Edwards RHT, Hill DK, Jones DA and Merton PA.** Fatigue of long duration in human skeletal muscle after exercise. *J Physiol* 272: 778, 1977.

31. **Ervasti JM and Campbell KP**. Membrane organization of the dystrophin-glycoprotein complex. *Cell* 66: 1121-1131, 1991.

32. **Fowles JR and Green HJ**. Coexistence of potentiation and low-frequency fatigue during voluntary exercise in human skeletal muscle. *Can J Physiol Pharmacol* 181: 1092-1100, 2003.

33. **Gallagher PJ, Herring BP and Stull JT**. Myosin light chain kinases. *J Muscle Res Cell Motil* 18: 1-16, 1997.

34. **Giorgi D, Brand-Arpon V and Rouquier S**. The functional myosin light chain kinase (MYLK) gene localizes with marker D3S3552 on human chromosome 3q21 in a >5-Mb yeast artificial chromosome region and is not linked to olfactory receptor genes. *Cytogenet Cell Genet* 92: 85-88, 2001.

35. **Giorgi D, Ferraz C, Mattéi MG, Demaille J and Rouquier S**. The myosin light chain kinase gene is not duplicated in mouse: partial structure and chromosomal localization of Mylk. *Genomics* 75: 49-56, 2001.

36. **Gonzalez B, Negredo P, Hernando R and Manso R**. Protein variants of skeletal muscle regulatory myosin light chain isoforms: prevalence in mammals, generation and transitions during muscle remodeling. *Eur J Physiol* 443: 377-386, 2002.

37. **Gonzalez E, Messi ML and Delbono O**. Specific force of single intact extensor digitorum longus and soleus mouse muscle fibers declines with aging. *J Membr Biol* 178: 175-183, 2000.

38. **Gordon AM, Homsher E and Regnier M**. Regulation of contraction in striated muscle. *Physiol Rev* 80: 853-924, 2000.

39. **Grange RW, Vandenboom R and Houston ME**. Physiological significance of myosin phosphorylation in skeletal muscle. *Can J Appl Physiol* 18: 229-242, 1993.

40. **Grange RW, Vandenboom R, Xeni J and Houston ME**. Potentiation of in vitro concentric work in mouse fast muscle. *J Appl Physiol* 84: 236-243, 1998.

41. **Hamilton SL, Serysheva I and Strasburg GM**. Calmodulin and excitation-contraction coupling. *News Physiol Sci* 15: 281-284, 2000.

42. **Harris JB and Johnson MA**. Further observations on the pathological responses of rat skeletal muscle to toxins isolated from the venom of the Australian tiger snake, Notechis scutatus scutatus. *Clin Exp Pharmacol Physiol* 5: 587-600, 1978.

43. **Head SI**. Membrane potential, resting calcium and calcium transients in isolated muscle fibres from normal and dystrophic mice. *J Physiol* 469: 11-19, 1993.

44. **Head SI, Williams DA and Stephenson DG**. Abnormalities in structure and function of limb skeletal muscle fibres of dystrophic *mdx* mice . *Proc R Sot Lond B BioZ Sci* 248: 163-169, 1992.

45. **Hidalgo C, Craig R, Ikebe M and Padron R**. Mechanism of phosphorylation of the regulatory light chain of myosin from tarantula striated muscle. *J Muscle Res Cell Motil* 22: 51-59, 2001.

46. **Hill CA, Thompson MW, Ruell PA, Thom JM and White MJ**. Sarcoplasmic reticulum function and muscle contractile character following fatiguing exercise in humans. *J Physiol* 531: 871-878, 2001.

47. **Hirsh JK, Searl TJ and Silinsky EM**. Regulation by Rab3A of an Endogenous Modulator of Neurotransmitter Release at Mouse Motor Nerve Endings. *J Physiol* 545: 337-343, 2002.

48. **Hopf FW, Turner PR, Denetclaw WF, Reddy P and Steinhardt RA**. A critical evaluation of resting intracellular free calcium regulation in dystrophic *mdx* muscle. *Am J Physiol* 271: C1325-C1339, 1996.

49. **Houston ME, Green HJ and Stull JT**. Myosin light chain phosphorylation and isometric twitch potentiation in intact human muscle. *Pfluegers Arch* 403: 352, 1985.

50. **Ibraghimov-Beskrovnaya O, Ervasti JM, Leveille CJ, Slaughter CA, Sernett SW and Campbell KP**. Primary structure of dystrophin-associated glycoproteins linking dystrophin to the extracellular matrix. *Nature* 355: 696-702, 1992.

51. **Jiang Y and Julian FJ**. Effects of ramp shortening during linear phase of relaxation on $[Ca^{2+}]_i$ in intact skeletal muscle fibers. *Am J Physiol* 276: C152-C160, 1999.

52. **Jones DA**. High-and low-frequency fatigue revisited. *Acta Physiol Scand* 156: 265-270, 1996.

53. **Karpati G, Carpenter S and Prescott S**. Small-caliber skeletal muscle fibers do not suffer necrosis in *mdx* mouse dystrophy. *Muscle Nerve* 11: 795-803, 1988.

54. **Koenig M, Hoffman EP, Bertelson CJ, Monaco AP, Feener C and Kunkel LM**. Complete cloning of the Duchenne muscular dystrophy (DMD) cDNA and preliminary genomic organization of the DMD gene in normal and affected individuals. *Cell* 50: 509-517, 1987.

55. **Krarup C**. Enhancement and diminution of mechanical tension evoked by staircase and by tetanus in rat muscle. *J Physiol* 311: 355-372, 1981.

56. **Lännergren J, Bruton JD and Westerblad H**. Vacuole formation in fatigued skeletal muscle fibres from frog and mouse: effects of extracellular lactate. *J Physiol* 526: 597-611, 2000.

57. **Lännergren J and Westerblad H**. The temperature dependence of isometric contractions of single, intact fibres dissected from a mouse foot muscle. *J Physiol* 390: 285-293, 1987.

58. **Levitsky DI**. Actomyosin Systems of Biological Motility. *Biochemistry (Mosc)* 69: 1177-1189, 2004.

59. **Linari M, Dobbie I, Reconditi M, Koubassova N, Irving M, Piazzesi G and Lombardi V**. The stiffness of skeletal muscle in isometric contraction and rigor: the fraction of myosin heads bound to actin. *Biophys J* 74: 2459-2473, 1998.

60. **Lynch GS, Hinkle RT, Chamberlain JS, Brooks SV and Faulkner JA**. Force and power output of fast and slow skeletal muscles from *mdx* mice 6-28 months old. *J Physiol* **535**: 591-600, 2001.

61. **Lynch GS, Rafael JA, Hinkle RT, Cole NM, Chamberlain JS and Faulkner JA**. Contractile properties of diaphragm muscle segments from old *mdx* and old transgenic *mdx* mice. *Am J Physiol* 272: C2063-C2068, 1997.

62. **MacIntosh BR**. Role of calcium sensitivity modulation in skeletal muscle performance. *News Physiol Sci* 18: 222-225, 2003.

63. **Mallouk N, Jacquemond V and Allard B**. Elevated subsarcolemmal Ca^{2+} in *mdx* mouse skeletal muscle fibers detected with Ca^{2+}-activated K^+ channels. *Proc Natl Acad Sci U S A* 97: 4950-4955, 2000.

64. **Manning DR and Stull JT**. Myosin light chain phosphorylation and phosphorylase A activity in rat extensor digitorum longus muscle. *Biochem Biophys Res Commun* 90: 164-170, 1979.

65. **Manning DR and Stull JT**. Myosin light chain phosphorylation-dephosphorylation in mammalian skeletal muscle. *Am J Physiol Cell Physiol* 242: C234-C241, 1982.

66. **Marchenko V and Rogers RF**. Selective loss of high-frequency oscillations in phrenic and hypoglossal activity in the decerebrate rat during gasping. *Am J Physiol Regul Integr Comp Physiol* 291: R1414-R1429, 2006.

67. **Matsuda R, Spector D and Strohman RC**. Regenerating adult chicken skeletal muscle and satellite cell cultures express embryonic patterns of myosin and tropomyosin isoforms. *Dev Biol* 100: 478-488, 1983.

68. **Mattson JP, Millerm TA, Poole DC and Delp MD**. Fiber composition and oxidative capacity of hamster skeletal muscle. *J Histochem Cytochem* 50: 1685-1692, 2002.

69. **Melloni E, Michetti M, Salamino F, Sparatore B and Pontremoli S**. Mechanism of action of a new component of the Ca(2+)-dependent proteolytic system in rat brain: the calpain activator. *Biochem Biophys Res Commun* 249: 583-588, 1998.

70. **Metzger JM, Greaser ML and Moss RL**. Variations in cross-bridge attachment rate and tension with phosphorylation of myosin in mammalian skinned skeletal muscle fibers. *J Gen Physiol* 93: 855-883, 1989.

71. **Michetti M, Viotti PL, Melloni E and Pontremoli S.** Mechanism of action of the calpain activator protein in rat skeletal muscle. *Eur J Biochem* 202: 1177-1180, 1991.

72. **Mizuno M and Secher NH.** Histochemical characteristics of human expiratory and inspiratory intercostal muscles. *J Appl Physiol* 67: 592-598, 1989.

73. **Moens P, Baatsen PHWW and Marechal G.** Increased susceptibility of EDL muscles from *mdx* mice to damage induced by contractions with stretch. *J Muscle Res Cell Motil* 4: 451, 1993.

74. **Moore RL, Houston ME, Iwamoto GA and Stull JT.** Phosphorylation of rabbit skeletal muscle myosin in situ. *J Cell Physiol* 125: 301-305, 1985.

75. **Moore RL and Stull JT.** Myosin light chain phosphorylation in fast and slow skeletal muscles in situ. *Am J Physiol* 247: C462-C471, 1984.

76. **Ogilvie RW and Feeback DL.** A metachromatic dye-ATPase method for the simultaneous identification of skeletal muscle fiber types I, IIA, IIB and IIC. *Stain Technol* 65: 231-241, 1990.

77. **Pastoret C and Sebille A.** Time course study of the isometric contractile properties of *mdx* mouse striated muscles. *J Muscle Res Cell Motil* 14: 423-431, 1993.

78. **Petrof BJ, Shrager JB, Stedman HH, Kelly AM and Sweeney HL.** Dystrophin protects the sarcolemma from stresses developed during muscle contraction. *Proc Natl Acad Sci USA* 90: 3710-3714, 1993.

79. **Petrof BJ, Stedman HH, Shrager JB, Eby J, Sweeney HL and Kelly AM.** Adaptations in myosin heavy chain expression and contractile function in dystrophic mouse diaphragm. *Am J Physiol* 265: C834-C841, 1993.

80. **Rassier DE and MacIntosh BR.** Coexistence of potentiation and fatigue in skeletal muscle. *Braz J Med Biol Res* 33: 499-508, 2000.

81. **Rassier DE and MacIntosh BR.** Sarcomere length-dependence of activity-dependent twitch potentiation in mouse skeletal muscle. *BMC Physiol* 10: 19, 2002.

82. **Renganthan M, Messi ML and Delbono O**. Overexpression of IGF-1 exclusively in skeletal muscle prevents age-related decline in the number of dihydropyridine receptors. *J Biol Chem* 273: 28845-28851, 1998.

83. **Rezvani M, Cafarelli E and Hood DA**. Performance and excitability of *mdx* mouse muscle at 2, 5, and 13 wk of age. *J Appl Physiol* 78: 961-967, 1995.

84. **Rideau Y, Jankowski LW and Grellet J**. Respiratory function in the muscular dystrophies. *Muscle Nerve* 4: 155-164, 1981.

85. **Rijkelijkhuizen JM, De Ruiter CJ, Huijing PA and de Haan A**. Low-frequency fatigue, post-tetanic potentiation and their interaction at different muscle lengths following eccentric exercise. *J Exp Biol* 208: 55-63, 2005.

86. **Rivero JL, Talmadge RJ and Edgerton VR**. Interrelationships of myofibrillar ATPase activity and metabolic properties of myosin heavy chain-based fibre types in rat skeletal muscle. *Histochem Cell Biol* 111: 277-287, 1999.

87. **Rosenfeld SS and Taylor EW**. Kinetic studies of calcium and magnesium binding to troponin. *J Biol Chem* 260: 242-251, 1985.

88. **Ryder JW, Lau KS, Kamm KE and Stull JT**. Enhanced skeletal muscle contraction with myosin light chain phosphorylation by a calmodulin-sensing kinase. *J Biol Chem* 282: 20447-20454, 2007.

89. **Sacco P, Jones DA, Dick JR and Vrbova G**. Contractile properties and susceptibility to exercise-induced damage of normal and *mdx* mouse tibialis anterior muscle. *Clin Sci (Lond)* 82: 227-236, 1992.

90. **Salamino F, Sparatore B, Melloni E, Michetti M, Viotti PL, Pontremoli S and Carafoli E**. The plasma membrane calcium pump is the preferred calpain substrate within the erythrocyte. *Cell Calcium* 15: 28-35, 1994.

91. **Sale D**. Postactivation potentiation: role in performance. *Br J Sports Med* 38: 386-387, 2004.

92. **Schacterle GR and Pollack RL**. A simplified method for the quantitative assay of small amounts of protein in biologic material. *Anal Biochem* 51: 654-655, 1973.

93. **Schwaller B, Dick J, Dhoot G, Carroll S, Vrbova G, Nicotera P, Pette D, Wyss A, Bluethmann H, Hunziker W and Celio MR**. Prolonged contraction-relaxation cycle of fast-twitch muscles in parvalbumin knockout mice. *Am J Physiol* 276: 395-403, 1999.

94. **Sicinski P, Geng Y, Ryder-Cook AS, Barnard EA, Darlison MG and Barnard PJ**. The molecular basis of muscular dystrophy in the *mdx* mouse: a point mutation. *Science* 244: 1578-1580, 2006.

95. **Spencer MJ, Walsh CM, Dorshkind KA, Rodriguez EM and Tidball JG**. Myonuclear apoptosis in dystrophic *mdx* muscle occurs by perforin-mediated cytotoxicity. *J Clin Invest* 99: 2745-2751, 1997.

96. **Staron RS, Kraemer WJ, Hikida RS, Fry AC, Murray JD and Campos GE**. Fiber type composition of four hind limb muscles of adult Fisher 344 rats. *Histochem Cell Biol* 111: 117-123, 1999.

97. **Stedman HH, Sweeney HL, Shrager JB, Maguire HC, Panettieri RA, Petrof BJ, Narusawa M, Leferovich JM, Sladkey JT and Kelly AM**. The *mdx* mouse diaphragm reproduces the degenerative changes of Duchenne muscular dystrophy. *Nature* 352: 536-539, 1991.

98. **Stevens ED and Faulkner JA**. The capacity of *mdx* mouse diaphragm to do oscillatory work. *J Physiol* 522: 457-466, 2000.

99. **Street SF**. Lateral transmission of tension in frog myofibers: a myofibrillar network and transverse cytoskeletal connections are possible transmitters. *J Cell Physiol* 114: 346-364, 1983.

100. **Swash M and Schwartz MS**. *Neuromuscular Diseases: A Practical Approach to Diagnosis and Management* . Great Britain: Springer-Verlag London Ltd, 2006.

101. **Sweeney HL, Bowman BM and Stull JT**. Myosin light chain phosphorylation in vertebrate striated muscle: regulation and function. *Am J Physiol* 264: C1085-C1095, 1993.

102. **Sweeney HL and Stull JT**. Alteration of cross-bridge kinetics by myosin light chain phosphorylation in rabbit skeletal muscle: implications for regulation of actin-myosin interaction. *Proc Natl Acad Sci U S A* 87: 414-418, 1990.

103. **Tidball JG, Albrecht DE, Lokensgard BE and Spencer MJ**. Apoptosis precedes necrosis of dystrophin-deficient muscle. *J Cell Sci* 108: 2197-2204, 1995.

104. **Turner PR, Fong PY, Denetclaw WF and Steinhardt RA**. Increased calcium influx in dystrophic muscle. *J Cell Biol* 115: 1701-1712, 1991.

105. **Turner PR, Schultz R, Ganguly B and Steinhardt RA**. Proteolysis results in altered leak channel kinetics and elevated free calcium in *mdx* muscle. *J Membr Biol* 133: 243-251, 1993.

106. **Turner PR, Westwood T, Regen CM and Steinhardt RA**. Increased protein degradation results from elevated free calcium levels found in muscle from *mdx* mice. *Nature Lond* 335: 735-738, 1988.

107. **Tutdibi O, Brinkmeier H, Rüdel R and Föhr KJ**. Increased calcium entry into dystrophin-deficient muscle fibres of MDX and ADR-MDX mice is reduced by ion channel blockers. *J Physiol* 515: 859-868, 1999.

108. **Vandenboom R, Grange RW and Houston ME**. Myosin phosphorylation enhances rate of force development in fast-twitch skeletal muscle. *Am J Physiol* 268: C596-C603, 1995.

109. **Vandenboom R and Houston ME**. Phosphorylation of myosin and twitch potentiation in fatigued skeletal muscle. *Can J Physiol Pharmacol* 74: 1315-1321, 1996.

110. **Vandenboom R, Xeni J, Bestic NM and Houston ME**. Increased force development rates of fatigued mouse skeletal muscle are graded to myosin light chain phosphate content. *Am J Physiol Regul Integr Comp Physiol* 272: 1980-1984, 1997.

111. **Watchko JF, Hoffman EP and O'Day TL**. Functional characteristics of dystrophic skeletal muscle: insights from animal models. *J Appl Physiol* 93: 407-417, 2002.

112. **Webster C, Silberstein L, Hays AP and Blau HM**. Fast muscle fibers are preferentially affected in Duchenne muscular dystrophy. *Cell* 52: 503-513, 1988.

113. **Westerblad H, Duty S and Allen DG**. Intracellular calcium concentration during low-frequency fatigue in isolated single fibers of mouse skeletal muscle. *J Appl Physiol* 75: 382-388, 1993.

114. **Whalen RG, Sell SM, Butler-Browne GS, Schwarz K, Bouveret P and Pinset-Harstrom I**. Three myosin heavy chain isozymes appear sequentially in rat muscle development. *Nature* 292: 805-809, 1981.

115. **Williams DA, Head SI, Lynch GS and Stephenson DG**. Contractile properties of skinned muscle fibres from young and adult normal and dystrophic (*mdx*) mice. *J Physiol* 460: 51-67, 1993.

116. **Wolff AV, Niday AK, Voelker KA, Call JA, Evans NP, Granata KP and Grange RW**. Passive mechanical properties of maturing extensor digitorum longus are not affected by lack of dystrophin. *Muscle Nerve* 34: 304-312, 2006.

117. **Woods CE, Novo D, DiFranco M and Vergara JL**. The action potential-evoked sarcoplasmic reticulum calcium release is impaired in mdx mouse muscle fibres. *J Physiol* 557: 59-75, 2004.

118. **Zhi G, Ryder JW, Huang J, Ding P, Chen Y, Zhao Y, Kamm KE and Stull JT**. Myosin light chain kinase and myosin phosphorylation effect frequency-dependent potentiation of skeletal muscle contraction. *Proc Natl Acad Sci U S A* 102: 17519-17524, 2005.

119. **Zychlinsky A, Zheng LM, Liu CC and Young JD**. Cytolytic lymphocytes induce both apoptosis and necrosis in target cells. *J Immunol* 146: 393-400, 1991.